Chapter 2
Multi-Wavelength WDM Fiber Laser

In this chapter, we demonstrate a multi-wavelength wavelength-division-multiplexed(WDM) continuous-wave(CW) fiber laser by utilizing the theorem of Fabry-Pérot resonance. The multi-wavelength fiber laser can be in application of many different purposes [15-18]. We use the fiber loop mirror to form a cavity in our laser system, and a 1.3 μm semiconductor optical amplifier (SOA) also be used as a gain material in the cavity. If we want to launch a 1.5 μm laser, we can utilize a 1.5 μm SOA to substitute for the 1.3μm SOA. Besides, our fiber laser can be extensively applied to carrying electrical subcarriers in optical communication systems by placing a phase modulator (PM) into our laser system. Comparing with the theoretical model, our experimental results show well coincidence with the theoretical model. With our setup, we can launch a very stable laser by this structure. Moreover, according to our measure results, the output side-mode suppression ration (SMSR) of our laser is large. Therefore, we can put our symmetrical laser in use in the fiber-optic communication system.

In the first section, we will describe the structure of our symmetric resonator laser system. The theoretical model will be derived in section 2-2. We also give numerical calculation results of the theoretical model in the same section. In section 2-3, we set up the experimental architecture and analyze the research results containing the condition of the variation of lasing power, SMSR and the variation of polarization state. A summary is

given in section 2-4 finally.

2-1 The Structure of the Multi-Wavelength Fiber Resonator Laser

Multi-wavelength fiber laser has been demonstrated for many years [19]. Multi-wavelength fiber laser source attracts lots of interests due to its potential applications and low cost in optical instrument test, WDM technique, and optical sensing or measurement equipment.

2-1-1 Broadband SOA in the Resonator Laser

Fiber resonator laser source employing a SOA as the gain medium are appealing due to the potential for low cost. The amplified spontaneous emission (ASE) light from a SOA was recently proposed as a suitable light source for multi-Gb/s speed WDM applications [20]. ASE light source are potentially attractive for cost-sensitive applications.

The fiber ring light source structure with SOA has been developed. Such a technique can apply to the density wavelength-division multiplexing (DWDM) [21]. In addition to stable room temperature operation, the SOA has many advantages in the fiber resonator cavity, such as electrical pumping, easy gain tuning, its potential for operation at any wavelength where lasing is possible, broad bandwidth, very small size, the possibility of integration with other control circuits on a single chip and function upgrading and so on.

In our fiber resonator laser system, we use the gain parameter and ASE of SOA to produce the multi-wavelength WDM fiber laser. The basic

components of SOA include a SOA diode, a laser diode driver and a temperature controller. The main body SOA diode is a multiple quantum well structure and is made from Philips Inc.

The function of the laser diode driver is to tune the injecting current to excite the energy level of the multiple quantum well structure of the SOA diode. After the SOA diode being excited, the ASE phenomenon will ensue. With increasing the injection current, the peak power of ASE become higher and higher, and the peak wavelength of ASE will drift at the same time.

The temperature controller is put in use to keep the SOA diode from exceeding the temperature limitation of the working region of the SOA diode. The temperature controller has a characteristic of native resistor coefficient while the adjusted resistor value becomes higher than the limitation we set. The relationship between the resistor value and the operational temperature is linear in small adjusting range.

2-1-2 Description of The Experimental Setup

We applied the theorem of Fabry-Pérot resonators in our experimental system. We want to fabricate a fiber resonator laser by utilizing the laser round-trip oscillation in the cavity which was constructed from the fiber loop mirrors. As the schematic diagram shown in Fig. 2-1, the architecture of the fiber resonator laser consists of a 1.3 μm SOA, 1×4 channel WDM, 90:10 2×2 fiber couplers, and 50:50 1×2 fiber couplers. The 1×4 channel WDM with a channel spacing of 0.8 nm (100 GHz) operating around the 0.8 μm to 1.5 μm has been used in the fiber resonator cavity. The equivalent structure of the Fabry-Pérot resonator cavity made from the

all-fiber loop mirrors is shown in Fig. 2-2. From Fig. 2-2, we can describe some formula by the theory of resonator. The round-trip fiber loops are equal to mirrors R_i and R_j, respectively. Therefore, we apply the theory of general laser resonance with the fiber loop mirrors to describe this experimental structure.

For the sake of forming a fiber loop mirror as shown in Fig. 2-3, we connect the port 1 and port 2 of the fiber coupler with a fiber connector. The coupling coefficient of port 1 and port 2 are confirmed according to the signal input port. The light reflected by the fiber loop mirrors will be round-trip amplified by SOA. In our experiment, SOA plays an important role. It not only supplies laser source but also amplifies the gain profile continuously. The temperature of the SOA is stabilized at 23℃ during spectrum measurement with temperature controller. We use the laser diode driver to tune the injecting current of the SOA from 0 mA to 230 mA. We can measure the spectrum of output channel of optical fiber coupler with an optical spectrum analyzer (OSA).

2-2 Theory of General Laser Resonance

In this section, the theoretical E-Field models of cavity laser system with fiber loop mirror will be described. We utilize the formula of the fiber loop mirrors to calculate the E-Field models of the Fabry-Pérot resonator cavity. Then we use the derived E-Field model to calculate the frequency response and observe the influence of the gain of SOA on the frequency response.

2-2-1 E-Field Models of Symmetric Resonator Cavity

As shown in Fig. 2-3, we analyze the E-Field of the fiber loop mirror in our resonator optical cavity before us deriving the general formula of our resonator laser. After getting the E-Field formula of fiber loop mirror, we can then derive the general theoretical model of the resonator laser.

2-2-1-1 E-Field of the Fiber Loop Mirror

A fiber loop mirror is shown schematically in Fig. 2-3. The port 1 and port 2 of the fiber coupler are connected with each other by the fiber connector. Assuming that lightwave travels towards the coupler in port 3 and the coupling coefficient K = 0.5. Therefore, in ideal condition, fifty percent of the input light travels counterclockwise around the fiber loop and the other fifty percent travels clockwise around the fiber loop. Light coupled across the waveguides of the coupler suffers a $\pi/2$ phase lag while the light traveling through the waveguide straightly and this can be found from Eq. 2-1. For that reason, the transmitted intensity in port 4 is the sum of a clockwise field of arbitrary phase φ and a counterclockwise field of relative phase $\varphi-\pi$ with both of equal amplitude. This results in a zero transmitted intensity and all input light is reflected back along the input port 3 by considering the conservation of energy. The above description is very much idealized. In practice, the splitting ratio of the coupler may not be exactly 50 percent at the required wavelength. There will be coupler excess loss, fiber loss, and birefringence in the fiber loop, etc.

In practice condition, the input power is reflected and transmitted by the fiber loop mirror. By using coupled mode theory, the relationship

between input and output amplitudes of the coupler can be expressed as [22]:

$$\begin{bmatrix} E_{1x,y} \\ E_{2x,y} \end{bmatrix} = \sqrt{(1-\gamma)} \begin{bmatrix} \sqrt{1-K_{x,y}} & j\sqrt{K_{x,y}} \\ j\sqrt{K_{x,y}} & \sqrt{1-K_{x,y}} \end{bmatrix} \begin{bmatrix} E_{3x,y} \\ 0 \end{bmatrix} \qquad (2\text{-}1)$$

where $K_{x,y}$ are the coupling coefficients for x- and y-polarized fundamental mode, γ is the intensity loss of the coupler which typically will be 5-10%, $E_{ix,y}$ (i = 1, 2, 3, 4) are the field amplitudes of x- and y-polarized modes, respectively. The two fields $E_{1x,y}$ and $E_{2x,y}$ travel around the loop in opposite directions. Taking the birefringence effect into account, the x and y components of each field may experience different optical path lengths and attenuation. The birefringence in the fiber loop may arise from bending or twisting in the fiber, or from one or more discrete optical elements, etc. These optical characteristics of the fiber loop mirror can be represented by an equivalent waveplate with retardation $\mathbf{\Delta}$ and orientated at an angle of θ [23]. Moreover, they also can be represented by equivalent Jones matrices $[J_C]$ and $[J_A]$ for the clockwise and counterclockwise paths, respectively. Considering reciprocal propagation, the $[J_C]$ and $[J_A]$ are related by $[\tilde{J}_C] = [J_A]$, where $[\tilde{J}_C]$ is the transpose of $[J_C]$ and $[\tilde{J}_C] = [J_C]$ [23]. The relationship between the elements of the Jones matrix and a waveplate, which has retardation Δ and is orientated at an angle of θ, is derived in Appendix Ⅰ.

With the analysis above and from Eq. 2-1, we can derive the $E_{1x,y}'$ and $E_{2x,y}'$ as :

$$\begin{bmatrix} E_{2x}' \\ E_{2y}' \end{bmatrix} = [J_C] \begin{bmatrix} -E_{2x} \\ E_{2y} \end{bmatrix} e^{(-\alpha + j\beta)L} \tag{2-2}$$

and

$$\begin{bmatrix} -E_{1x}' \\ E_{1y}' \end{bmatrix} = [J_A] \begin{bmatrix} E_{1x} \\ E_{1y} \end{bmatrix} e^{(-\alpha + j\beta)L} \tag{2-3}$$

where

$$[J_C] = \begin{bmatrix} J_{xx} & J_{xy} \\ J_{yx} & J_{yy} \end{bmatrix}$$

(2-4)

is the Jones matrix for clockwise optical path, and

$$[J_A] = \begin{bmatrix} J_{xx} & J_{yx} \\ J_{xy} & J_{yy} \end{bmatrix} \tag{2-5}$$

is the Jones matrix for counterclockwise optical path, respectively. The elements of $[J_C]$ and $[J_A]$ are defined as Appendix Ⅰ. Moreover, α is the field loss coefficient, β is the propagation constant and L is the fiber loop length. Then, the $E_{1x,y}'$ and $E_{2x,y}'$ propagate through the fiber coupler again and we can get the output fields $E_{3x,y}'$ and $E_{4x,y}'$:

$$\begin{bmatrix} E_{3x,y}' \\ E_{4x,y}' \end{bmatrix} = \sqrt{(1-\gamma)} \begin{bmatrix} \sqrt{1-K_{x,y}} & j\sqrt{K_{x,y}} \\ j\sqrt{K_{x,y}} & \sqrt{1-K_{x,y}} \end{bmatrix} \begin{bmatrix} E_{2x,y}' \\ E_{1x,y}' \end{bmatrix} \tag{2-6}$$

Then

$$\begin{bmatrix} E_{3x}' \\ E_{3y}' \\ E_{4x}' \\ E_{4y}' \end{bmatrix} = (1-\gamma) e^{(-\alpha + j\beta)L} \begin{bmatrix} A & B \\ C & D \end{bmatrix} \begin{bmatrix} E_{3x} \\ E_{3y} \\ 0 \\ 0 \end{bmatrix} \tag{2-7}$$

where the submatrixes A, B, C, D are defined as:

$$[A]=\begin{bmatrix} -2j\sqrt{1-K_x}\sqrt{K_x}J_{xx} & j[\sqrt{K_x}\sqrt{1-K_y}J_{xy}-\sqrt{1-K_x}\sqrt{K_y}J_{yx}] \\ j[\sqrt{K_x}\sqrt{1-K_y}J_{xy}-\sqrt{1-K_x}\sqrt{K_y}J_{yx}] & 2j\sqrt{1-K_y}\sqrt{K_y}J_{yy} \end{bmatrix}$$

$$[B]=\begin{bmatrix} (2K_x-1)J_{xx} & -\sqrt{K_x}\sqrt{K_y}J_{xy}-\sqrt{1-K_x}\sqrt{1-K_y}J_{yx} \\ \sqrt{1-K_x}\sqrt{1-K_y}J_{xy}+\sqrt{K_x}\sqrt{K_y}J_{yx} & (1-2K_y)J_{yy} \end{bmatrix}$$

$$[C]=\begin{bmatrix} (2K_x-1)J_{xx} & \sqrt{1-K_x}\sqrt{1-K_y}J_{xy}+\sqrt{K_x}\sqrt{K_y}J_{yx} \\ -\sqrt{K_x}\sqrt{K_y}J_{xy}-\sqrt{1-K_x}\sqrt{1-K_y}J_{yx} & (1-2K_y)J_{yy} \end{bmatrix}$$

$$[D]=\begin{bmatrix} -2j\sqrt{1-K_x}\sqrt{K_x}J_{xx} & j[\sqrt{K_x}\sqrt{1-K_y}J_{xy}-\sqrt{1-K_y}\sqrt{K_x}J_{yx}] \\ j[\sqrt{K_x}\sqrt{1-K_y}J_{xy}-\sqrt{1-K_y}\sqrt{K_x}J_{yx}] & 2j\sqrt{1-K_y}\sqrt{K_y}J_{yy} \end{bmatrix}$$

By knowing the $E_{3x,y}'$ and $E_{4x,y}'$, we can derive the reflection coefficient r and transmission coefficient t. In many experiments, the generality of r and t which take detailed birefringence into account are cumbersome and will not be required [24]. We can simplify the representations of the reflection coefficient r and transmission coefficient t by taking conservation of energy for propagation through the fiber loop into account. Consider the clockwise propagation of the field and assume that the field on entry to the birefringence media is given by **E**. The exit field is therefore $[J_c]\mathbf{E}$ and the input and output powers are related by:

$$\tilde{E}E=(\tilde{J}_C E)(J_C E)=\tilde{E}(\tilde{J}_C^* J_C)E \tag{2-8}$$

For conservation of energy, the $\tilde{J}_C^* J_C$ term must be equal to the unit matrix [I]. Then

$$[I]=\begin{pmatrix} J_{xx}^* J_{xx}+J_{yx}^* J_{yx} & J_{xx}^* J_{xy}+J_{yx}^* J_{yy} \\ J_{xy}^* J_{xx}+J_{yy}^* J_{yx} & J_{xy}^* J_{xy}+J_{yy}^* J_{yy} \end{pmatrix} \tag{2-9}$$

Similarly, with consideration of the counterclockwise field, we can get

$$[I]=\begin{pmatrix} J_{xx}^{*}J_{xx}+J_{xy}^{*}J_{xy} & J_{xx}^{*}J_{yx}+J_{xy}^{*}J_{yy} \\ J_{yx}^{*}J_{xx}+J_{yy}^{*}J_{xy} & J_{yx}^{*}J_{yx}+J_{yy}^{*}J_{yy} \end{pmatrix} \quad (2\text{-}10)$$

Compare Eq. 2-10 with Eq. 2-9, we can obtain $|J_{xx}|^2 = |J_{yy}|^2$ and $|J_{xy}|^2 = |J_{yx}|^2$. Considering Eq. 2-9 or Eq. 2-10, we can express the transmittance and reflectance as [24]:

$$R = (1-\gamma)^2 e^{-2\alpha L} K(1-K)J \quad (2\text{-}11)$$

$$T = (1-\gamma)^2 e^{-2\alpha L}[1-K(1-K)J] \quad (2\text{-}12)$$

where $J=2(|J_{xx}|^2+1)-(J_{yx}^{*}J_{xy}+J_{xy}^{*}J_{yx})$. For the special case of the Jones matrix is symmetric, which represents a birefringence equivalent to a single discrete waveplate $J_{xy} = J_{yx}$. Then, the expression for J reduces to $4|J_{xx}|^2$. Now assume the birefringence appears as wave retardation with a fast axis oriented at 90°. Then from Eq. 2-7 to Eq. 2-12, we can derive simplifying expressions for common fiber loop mirror [24]:

$$t = (1-2K)(1-\gamma)e^{(-\alpha+j\beta)L} \quad (2\text{-}13)$$

$$jr = 2j\sqrt{K}\sqrt{1-K}\,(1-\gamma)\,e^{(-\alpha+j\beta)L} \quad (2\text{-}14)$$

$$R = r^{*}r = 4\,K(1-K)\,(1-\gamma)^2 e^{-2\alpha L} \quad (2\text{-}15)$$

$$T = t^{*}t = (1-2K)^2(1-\gamma)^2 e^{-2\alpha L} \quad (2\text{-}16)$$

$$A = 1-(R+T) = 1-(1-\gamma)^2 e^{-2\alpha L} \quad (2\text{-}17)$$

where the symbols are defined as below:

t: transmission coefficient

r: reflection coefficient

R: reflectance

T: transmittance

A: loss

K: coupling coefficient

For the resonance situation, there are two necessary requirements [22]. The first is

$$\beta L = 2m\pi - \frac{\pi}{2}, \quad m \in Z \tag{2-18}$$

The second requirement for resonance specifies the coupling ratio K:

$$K = (1-\gamma)e^{-2\alpha L} \tag{2-19}$$

By understanding the E-Field models of the fiber loop mirror, we can combine the E-Field models of the fiber loop mirror and the gain characteristic to get the general theoretical model of the symmetric resonator laser. We will derive the theoretical model in the next subsection.

Before deriving the theoretical model of the general resonator laser, we can discuss why we shall choose a 50:50 1×2 fiber coupler to form a fiber loop mirror at the left side in Fig. 2-1. In ideal condition, a fiber loop mirror constructed from a 50:50 fiber coupler results in zero transmission. However, thinking of the birefringence effect, the transmission of the 50:50 fiber loop mirror is not zero. From Eq. 2-11, we can plot the reflectance as a function of coupling ratio and birefringence which is represented by $|J_{xx}|^2$. The result is shown in Fig. 2-4. From Fig. 2-4, we can find that with considering the birefringence effect, the maximum value of the reflectance occurs at the coupling ratio is equal to 0.5. In other words, the larger reflectance means the larger reflection output power of the signal. Therefore, we choose a 50:50 fiber coupler to form a fiber loop mirror at the left hand side.

Besides, we can plot the transmittance as a function of coupling ratio

and birefringence. The result is shown in Fig. 2-5. From Fig. 2-5, we can observe that the maximum value of the transmittance occurs at the coupling ratio being equal to 0 or 1. Therefore, we choose a 90:10 fiber coupler to form a fiber loop mirror at the right hand side in Fig. 2-1 to get the larger lasing output power.

2-2-1-2 General Theoretical Model of the Symmetric Resonator Laser

Combine the E-Field models of a single fiber loop mirror which was discussed in last subsection with the gain characteristic of the gain material in the resonator cavity, we now start to derive the general theoretical model of the symmetric resonator laser with two fiber loop mirrors.

The schematic diagram of the symmetric resonator laser with two fiber loop mirrors and the gain material is shown in Fig. 2-6. We define the one round-trip gain parameter G as:

$$G = g \times e^{(-\alpha_g + j\beta)L_2} \tag{2-20}$$

where g is the gain profile of the SOA and is a function of wavelength. Moreover, we define the one round-trip field loss coefficient of the WDM MUX and DeMUX as:

$$\alpha_{Wij} = \alpha_{Wi} \times \alpha_{Wj} \tag{2-21}$$

As derived from last subsection, if the input amplitude of the electrical field is E_{in}, then from Eq. 2-13 to Eq. 2-14, we can find the output amplitude of the electrical field E_{out} as [22]:

$$E_{out} = t_i t_j E_{in} \alpha_{Wij} G - r_i r_j t_i t_j E_{in} \alpha_{Wij}{}^3 G^3 + t_i t_j (r_i r_j)^2 E_{in} \alpha_{Wij}{}^5 G^5 - \ldots\ldots \tag{2-22}$$

$$E_{out} = \frac{t_i t_j \alpha_{Wij} G}{1 + r_i r_j \alpha_{Wij}{}^2 G^2} E_{in} \tag{2-23}$$

where t_i and r_i are the transmission coefficient and reflection coefficient of the left hand side fiber loop mirror in Fig. 2-6, respectively. Moreover, t_j and r_j are the transmission coefficient and reflection coefficient of the right hand side fiber loop mirror in Fig. 2-6, respectively. Then the output power intensity can be given as:

$$I_{out} = |E_{out}|^2 = \left| \frac{t_i t_j \alpha_{Wij} G}{1 + r_i r_j \alpha_{Wij}{}^2 G^2} \right|^2 \times |E_{in}|^2 \tag{2-24}$$

then

$$I_{out} = \left(\frac{T_i T_j \alpha_{Wij}{}^2 g^2 e^{-2\alpha_g L_2}}{(1 + \sqrt{R_i R_j}\, \alpha_{Wij}{}^2 g^2 e^{-2\alpha_g L_2})^2 - 4\alpha_{Wij}{}^2 g^2 \sqrt{R_i R_j}\, e^{-2\alpha_g L_2} [\sin^2(\frac{\beta}{2}(L_1 + L_3))]} \right) I_{in} \tag{2-25}$$

and the detailed derivation is given in Appendix Ⅱ. Finally, the frequency response which is denoted as the transfer function H of the symmetric resonator laser with two fiber loop mirrors can be written as:

$$H = \frac{I_{out}}{I_{in}} = \left(\frac{T_i T_j \alpha_{Wij}{}^2 g^2 e^{-2\alpha_g L_2}}{(1 + \sqrt{R_i R_j}\, \alpha_{Wij}{}^2 g^2 e^{-2\alpha_g L_2})^2 - 4\alpha_{Wij}{}^2 g^2 \sqrt{R_i R_j}\, e^{-2\alpha_g L_2} [\sin^2(\frac{\beta}{2}(L_1 + L_3))]} \right) \tag{2-26}$$

Because of g being a function of wavelength, the transfer function H is a function of wavelength, too.

Eq. 2-26 expresses a symmetric resonator laser with two fiber loop mirrors. With our architecture, the general transfer function of the symmetric resonator laser with eight fiber loop mirrors can be written as:

$$H=\sum_{m,n}\left(\frac{T_{mi}T_{nj}\alpha_{Wm}\alpha_{Wn}g^{2}e^{-2\alpha_{g}L_{2}}}{(1+\sqrt{R_{mi}R_{nj}}\alpha_{Wm}\alpha_{Wn}g^{2}e^{-2\alpha_{g}L_{2}})^{2}-4\alpha_{Wm}\alpha_{Wn}g^{2}\sqrt{R_{mi}R_{nj}}e^{-2\alpha_{g}L_{2}}[\sin^{2}(\frac{\beta}{2}(L_{m1}+L_{n3}))]}\right) \quad (2\text{-}27)$$

where { m, n∈N; 1≦ m, n≦4}.

By using Eq. 2-26 and Eq. 2-27, we can simulate the optical response of the output laser exported from the symmetric fiber-loop-mirrors resonator cavity.

2-2-2 Numerical Results of Our Symmetric Resonator Laser

In section 2-2-1-2, we illustrate and analyze the E-field and the optical response of the symmetric resonator laser with a SOA and fiber loop mirrors in Eq. 2-22 and Eq. 2-25, respectively. In our experimental setup, we use a 1.3 μm SOA (Philips Inc. Model CQF882/E) as the gain material. The specification of the 1.3 μm SOA is list in Table 2-1. As shown in Fig. 2-7, we set up an experiment to measure the gain profile of the 1.3 μm SOA. We set the lasing power of the tunable laser equal to –25 dBm, the driving current of the SOA equal to 250 mA and the temperature of the SOA is controlled at 23℃. We use an isolator to protect the tunable laser from the reflected laser. The 1.3 μm SOA has a peak small-signal gain of 14.75 dBm at 1309 nm for an input signal power of –25 dBm when driven at a current $i_{SOA}=250$ mA. The optical spectrum of the gain profile of the 1.3 μm SOA when driven at the current $i_{SOA}=250$ mA is illustrated in Fig. 2-8. Furthermore, the variation of the peak value of the gain profile with

different driving current of the SOA is list in Table 2-2. With different SOA gain parameter G which is related to the driving current of the SOA, we show the numerical curves of the output optical response in Fig. 2-9. The optical responses of output lasing with the 1.3 μm SOA change as the driving current varies. From Fig. 2-9, we can find that the peak value of optical frequency response will increase when the gain parameter G of the SOA increases. Table 2-3 lists the calculation parameters of the fiber resonator laser.

2-3 Experimental Results of Our Symmetric Resonator Lasers

In this section, we would analysis the experimental results of the multi-wavelength WDM fiber laser with the semiconductor optical amplifier and the fiber loop mirrors. In our experiment, the fiber resonator cavity is composed of 1×4 WDM, a semiconductor optical amplifier, 1×2 optical fiber couplers and 2×2 optical fiber couplers and has been shown in Fig. 2-1. We analyze the lasing power, L-I curve and the stability of our designed symmetric resonator laser with various driving current of the SOA.

2-3-1 L-I Curve of Symmetric Resonator Laser with Different Driving Current of the SOA

We know that power loss is a serious problem in a long distance transmission. Hence the large range of the transmission power can increase the transmission distance. Therefore, it becomes more and more important

to increase the range of transmission power in a long distance optical transmission system. When the signal, which is injected into the transmission system, is modulated, the linear range of the L-I curve influences the transmission qualities, where L represents the peak power and I means to the driving current. Because when modulated signal is injected into this modulation system, we can get large range of output power at the output port. Therefore, the best condition of the L-I curve applied to transmission system is high linear range. From the general L-I curve of laser system, we can define the threshold current I_{th} and saturation current I_{sat}. Then the power range between I_{th} and I_{sat} is called linear range. When the linear range is broadened, the modulation depth will be increased. In our experimental structure, we utilize different value of the driving current to analyze the L-I curve of our symmetric resonator laser.

Beginning with the analysis, the relationship between the driving current of SOA and the output lasing power is discussed at first. The lasing power can be measured with an optical spectrum analyzer (Anritsu Model MS9710C). It is known to all that when the driving current exceeds the threshold current I_{th}, the lasing power increases rapidly with respect to enlarge a little of the driving current. Moreover, when the driving current exceeds saturation current I_{sat}, the lasing power does not become larger obviously and the lasing power becomes steady at last. In our experiment, we turn the driving current of the SOA from 0 mA to 230 mA, and the output lasing power increases gradually after the driving current exceeding the threshold current I_{th}.

In our WDM resonator system, there are four lasing wavelengths have

been demonstrated. Therefore, we measure and analyze their L-I curves respectively. In the experiment, we increase the driving current of the SOA and observe the variation of lasing power. The resultant L-I curves of the four wavelengths λ_1, λ_2, λ_3, λ_4 with different driving current are depicted in Fig. 2-10. From Fig. 2-10, we can find that while the driving current exceeds 60 mA, the four wavelengths λ_1, λ_2, λ_3, λ_4 start lasing. Moreover, from those results, we can find that the peak power of the output spectrum would increase as the driving current increasing. This means that the lasing phenomenon becomes more and more obvious. But as depicted in Fig. 2-10, we can find that the variation range of the peak power is decreased gradually while the driving current of SOA is increasing. This means the gain of the SOA is approaching saturation, and in our experiment the driving current is 250 mA while the gain saturation occurs.

2-3-2 Experimental Spectrum of the Symmetric Resonator Laser

As shown in Fig. 2-1, we utilize the fiber loop mirrors to form a symmetric resonator for the manipulation of the four wavelengths laser. We turn the driving current of the SOA from 0 mA to 230 mA, and the output lasing power increases gradually. The resultant output spectrum with which the driving current is equal to 90 mA, 130 mA, 170 mA and 210 mA is shown in Fig. 2-11 to Fig. 2-14, respectively. When the driving current of the SOA is 90 mA, the output lasing powers are –27.38 dBm, -26.6 dBm, -24.63 dBm and -24.99 dBm as shown in Fig. 2-11. As depicted in Fig. 2-12, the output lasing powers are –23.63 dBm, -22.73 dBm, -23 dBm and

-23.15 dBm when the driving current of the SOA is 130 mA. The output lasing powers are –22.27 dBm, -23.04 dBm, -22.21 dBm and -21.78 dBm, as shown in Fig. 2-13, when the driving current of the SOA is 170 mA. While the driving current of the SOA is 210 mA, the output lasing powers are –21.6 dBm, -21.76 dBm, -21.67 dBm and -21.11 dBm as depicted in Fig. 2-14.

Comparing Fig. 2-11 to Fig. 2-14 with Fig. 2-9, respectively, we can evidence that our experimental results are well consistent with the theoretical prediction. Besides, from Fig. 2-11 to Fig. 2-14, we can find that the output lasing powers become higher while the driving current of the SOA is turned larger. This is owing to the gain profile of the SOA described in section 2-2-2. As discussed in section 2-2-2, the peak power of the gain profile of the SOA becomes higher with respect to higher driving current. Therefore, while the driving current is turned larger, the output lasing power is higher amplified. Furthermore, from Fig. 2-11 to Fig. 2-14, we can observe that the peak power values of the four lasing wavelengths are getting more coincidence with each other when the driving current is turned larger. This will promote the qualities of the laser system.

After discussing the spectrum, we proceed to analyze the side mode suppression ratio (SMSR) of our laser. It is known that ASE noise and SMSR affect the transmission quality in an optical communication system [25-30]. If ASE noise is very large, the receiver signal is hard to be correctly filtered. When noise is effective reduced or the lasing power is increased, the value of signal to noise ratio (SNR) will be promoted and transmission quality should be increased. Therefore, a good transmission

system must confirm one condition that the SMSR has to be large. From above discussion, we measure the driving current versus SMSR curve of the four lasing wavelengths with different value of the driving current. The results are shown in Fig. 2-15, Fig. 2-16, Fig. 2-17 and Fig. 2-18, respectively. From Fig. 2-15 to Fig. 2-18, we can get a good value of SMSR of our symmetric resonator laser while the driving current of the SOA is turned larger. And the best value of SMSR is approximately 40 dBm. From those results, we know that the value of SMSR can be enlarged by changing the driving current of the SOA and we should produce four pure single mode lasers in our experimental structure.

2-3-3 Analysis of the Stability and the Power Variation of Our CW Laser

In the optical transmission system, the stability of output laser powers is very important because of its influences on the accuracy of transmission result. If the laser power is not stable, it will cause a great quantity loss of transmission data. For this reason, how to generate a stable laser becomes more and more important. The essential factor to stabilize fiber resonator laser is stabilizing its resonator cavity at first. In our experiment, we do our best to overcome the effects of the external unstable environment such as temperature, bending, stress and the swing of the optical fibers. Therefore, in our resonator laser system, we can generate four very stable wavelengths of output laser at λ = 1347.24 nm, λ = 1347.94 nm, λ = 1348.65 nm and λ = 1349.34 nm, respectively. We use the optical spectrum analyzer (OSA) to measure the variation of laser power. First, we fix the temperature of SOA

at 23℃ (R = 10 kΩ). Then, the lasing power of the resonator cavity with different driving current of the SOA is measured for one hour. Fig. 2-19(a), Fig. 2-20(a), Fig. 2-21(a) and Fig. 2-22(a) show the output spectrums while the SOA is driven at the current of 90 mA, 130 mA, 170 mA and 210 mA, respectively. Form those results we find that in this symmetric resonator cavity, we can get a stable laser.

The analysis of Fig. 2-19(a), Fig. 2-20(a), Fig. 2-21(a) and Fig. 2-22(a) are depicted in Fig. 2-19(b), Fig. 2-20(b), Fig. 2-21(b) and Fig. 2-22(b), respectively. Form Fig. 2-19(b), we observe the stability of lasing power can be controlled with $\triangle P < 0.3$ dBm while the driving current of the SOA is larger than 90 mA and the average of stability is about 0.17 dBm for λ_1, 0.15 dBm for λ_2 and λ_4, and 0.16 dBm for λ_3. Besides, form Fig. 2-20(b), we observe the stability of lasing power can be controlled with $\triangle P < 0.21$ dBm while the driving current of the SOA is larger than 130 mA and the average of stability is about 0.13 dBm for λ_1 and λ_3, 0.15 dBm for λ_2 and 0.11 dBm for λ_4. Moreover, form Fig. 2-21(b), we observe the stability of lasing power can be controlled with $\triangle P < 0.18$ dBm while the driving current of the SOA is larger than 170 mA and the average of stability is about 0.1 dBm for λ_1, λ_2, λ_3 and 0.08 dBm for λ_4. Furthermore, form Fig. 2-22(b), we observe the stability of lasing power can be controlled with $\triangle P < 0.09$ dBm while the driving current of the SOA is larger than 210 mA and the average of stability is about 0.05 dBm for λ_1 and λ_2, 0.04 dBm for λ_3 and 0.03 dBm for λ_4.

2-4 Polarization State Analysis of the Symmetric Laser

The polarization state analysis of laser source in the optical transmission system has been come into notice by the analyst. The unstable polarization state will influence the transmission quality and increase the bit error ratio (BER). Therefore, we must use some methods to compensate the polarization related penalties, such as the polarization mode dispersion (PMD), the polarization dependent loss (PDL), the polarization dependent gain (PDG) and the pulse duration modulation (PDM), which are all time-varying and un-predictable in fiber-optic systems. Besides, we must design a receiver to analyze the polarization states.

The polarization is related to the lasing power of the laser system in the experiment. In this section, we analyze the polarization state of our CW laser with varying the driving current of the SOA. We use the polarimeter (THORLABS Inc. Model PA430) to measure the polarization states of output lasing wavelengths for ten minutes while the SOA is driven at 90 mA, 130 mA, 170 mA and 210 mA. The results of polarization measurement at λ_1 = 1347.24 nm, λ_2 = 1347.94 nm, λ_3 = 1348.65 nm and λ_4 = 1349.34 nm are shown from Fig. 2-23 to Fig. 2-26, respectively. From these results we can obviously observe the trajectory of the polarization states. According to Fig. 2-23 to Fig. 2-26, we find the polarization state of our symmetric laser is very stable. Therefore our source is well fitting on the fiber-optic communication system. Moreover, we analyze the polarization state of lasing wavelengths with continuously turning the driving current from 80 mA to 250 mA. Fig. 2-27(a) to Fig. 2-27(d) show the experimental results. While the driving current of the SOA changes from 80 mA to 250 mA, the variations of the orientation of λ_1 = 1347.24

nm, λ_2 = 1347.94 nm, λ_3 = 1348.65 nm and λ_4 = 1349.34 nm are 15°, 14°, 12° and 10°, respectively. According to these results, the variations of polarization state are slightly influenced with the variation of the driving current of the SOA.

2-5 Summary

In this chapter, we successfully design a symmetric WDM fiber laser. In our experimental system, we can arbitrary change the driving current of the SOA. This driving current of the SOA influences the lasing power, SMSR, L-I curve, polarization state and so on. From our experimental result, we can produce a pure single mode laser with its SMSR approaching to 40 dBm and the lasing power is very stable which the △P can be controlled under 0.3 dBm while the driving current of the SOA is larger than 90 mA and △P can be controlled under 0.21 dBm while the driving current of the SOA is larger than 130 mA and △P can be controlled under 0.18 dBm while the driving current of the SOA is larger than 170 mA and △P can be controlled under 0.09 dBm while the driving current of the SOA is larger than 210 mA. Besides, we can find that the output lasing powers become higher while the driving current of the SOA is turned larger. From section 2-4, we can find that the polarization states of our lasers are stable. We can put our multi-wavelength WDM fiber laser in use in the fiber-optic communication system.

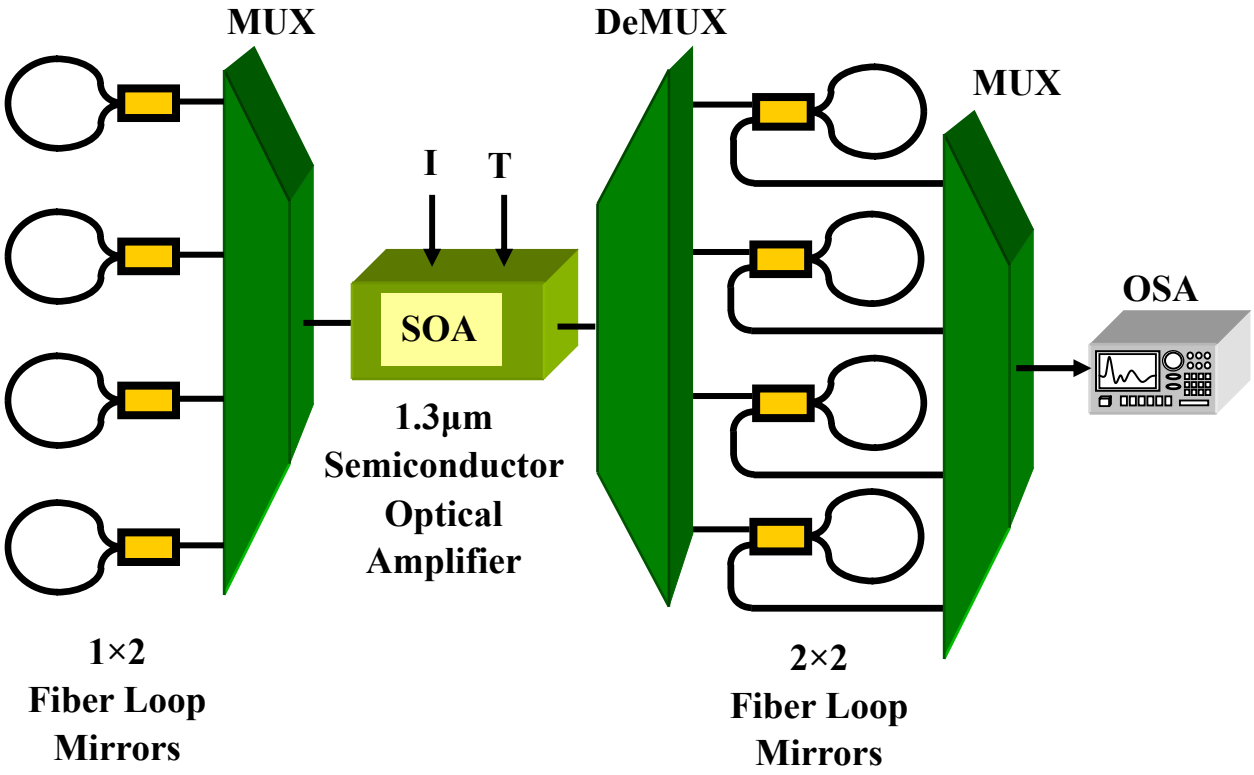

Fig. 2-1 The schematic diagram of the fiber ring laser architecture

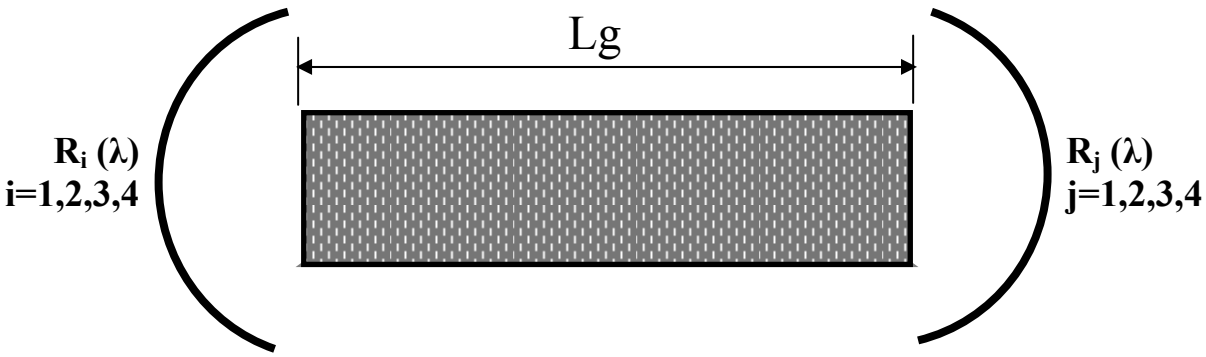

Fig. 2-2 The equivalent circuit of symmetric resonator fiber ring laser

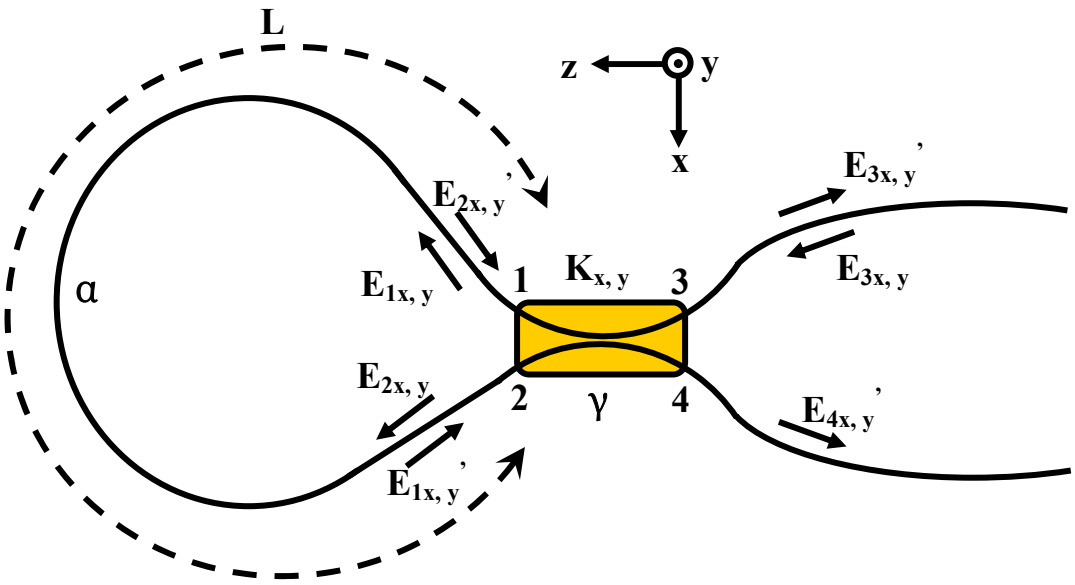

$K_{x,y}$：Coupling Coefficients for x- and y-polarized fundamental mode

γ：Intensity Loss of the Coupler

L：Fiber Loop Length

α：Field Loss Coefficient (Fiber Absorption)

Fig. 2-3 All-fiber loop mirror constructed from a fiber coupler

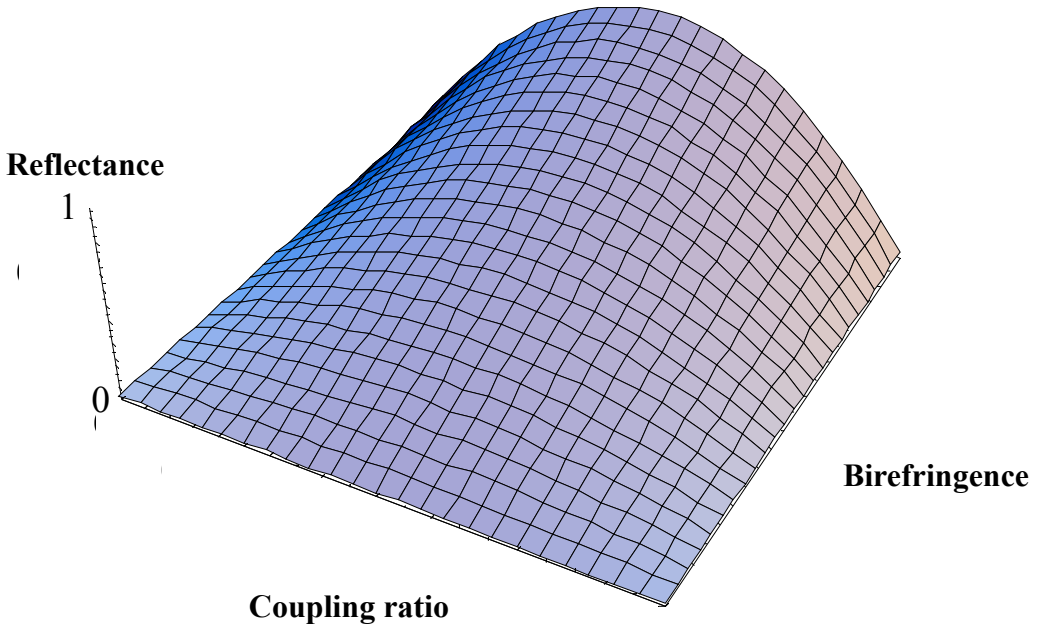

Fig. 2-4 The reflectance as a function of coupling ratio and birefringence of a fiber loop mirror

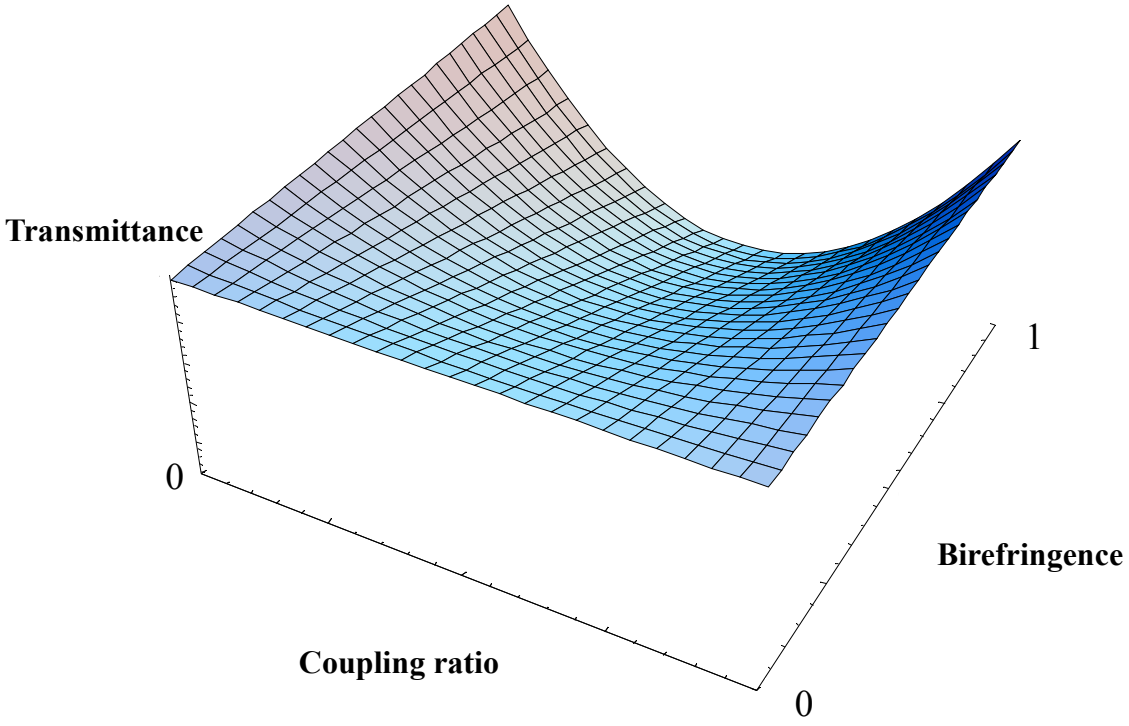

Fig. 2-5 The transmittance as a function of coupling ratio and birefringence of a fiber loop mirror

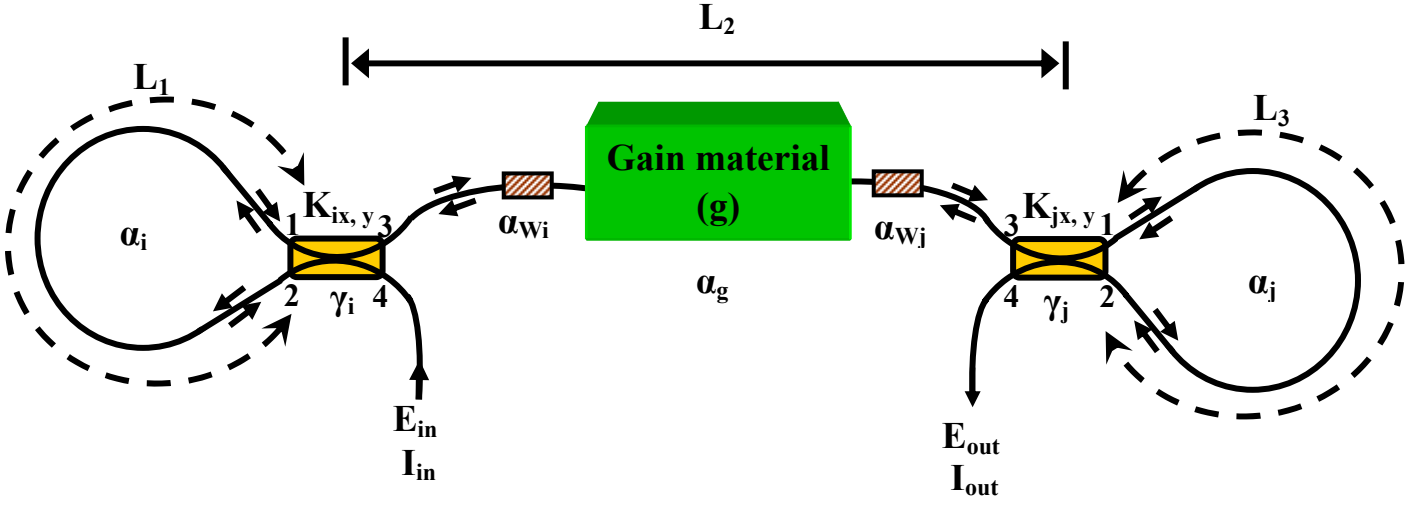

Fig. 2-6 The fiber laser with all-fiber loop mirror

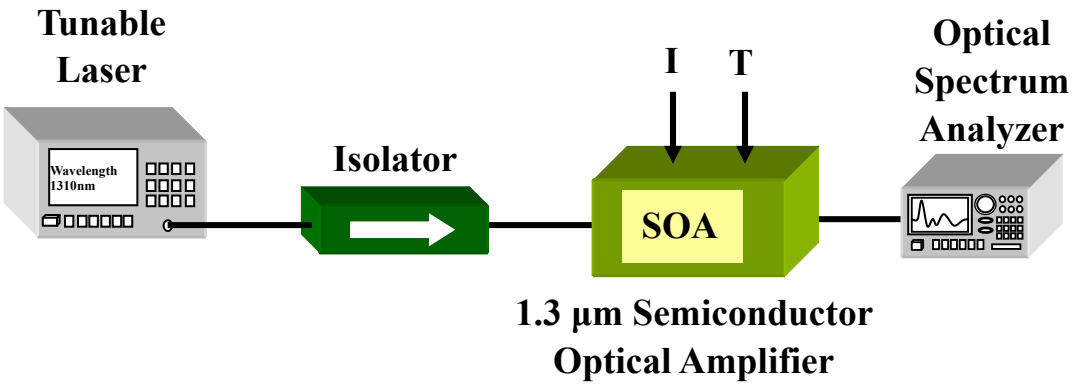

I：Laser Diode Driver

T：Temperature Controller

Fig. 2-7 Experimental setup of the gain profile measurement of the SOA at $i_{SOA}=250\text{mA}$

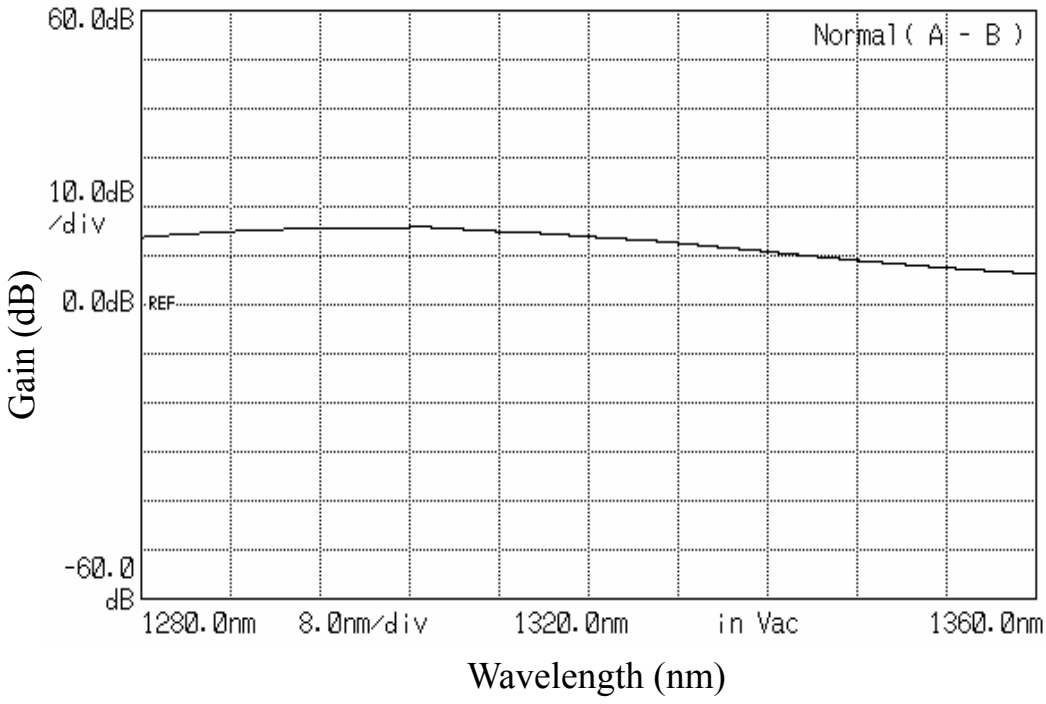

Fig. 2-8 The gain profile of the 1.3μm SOA at $i_{SOA}=250\text{mA}$

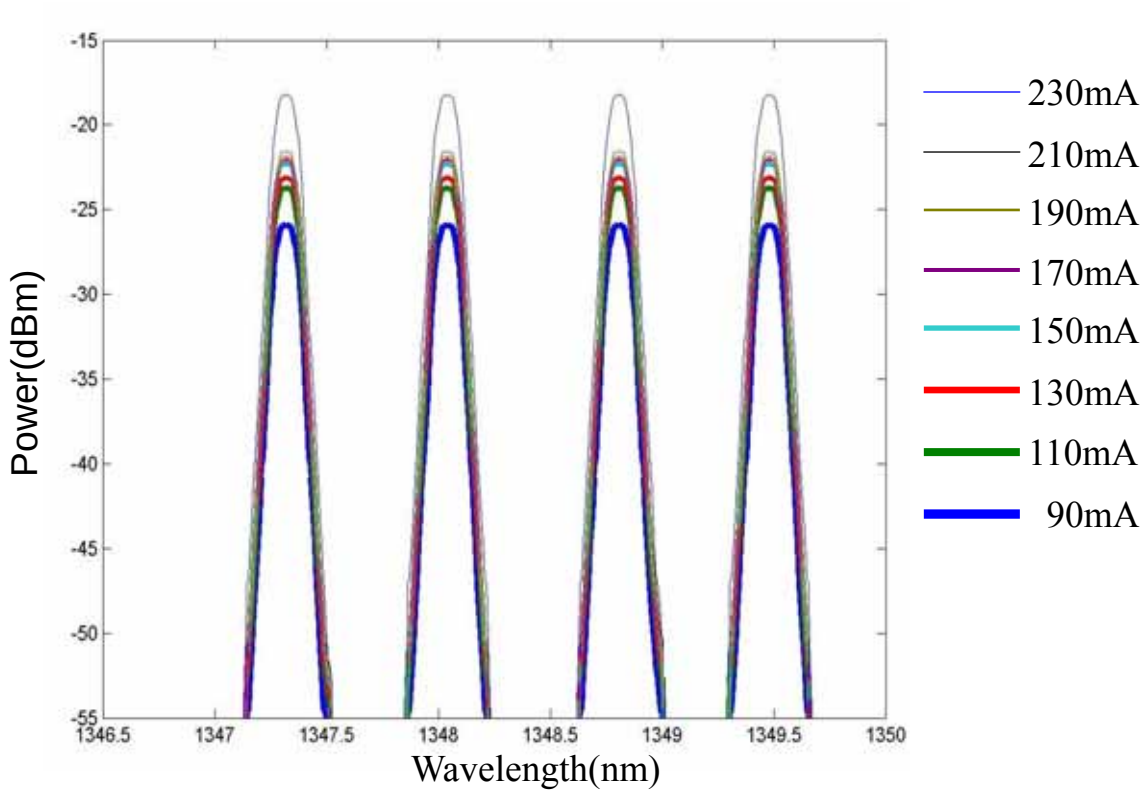

Fig. 2-9 The calculation results of the optical response of the output symmetric resonator laser

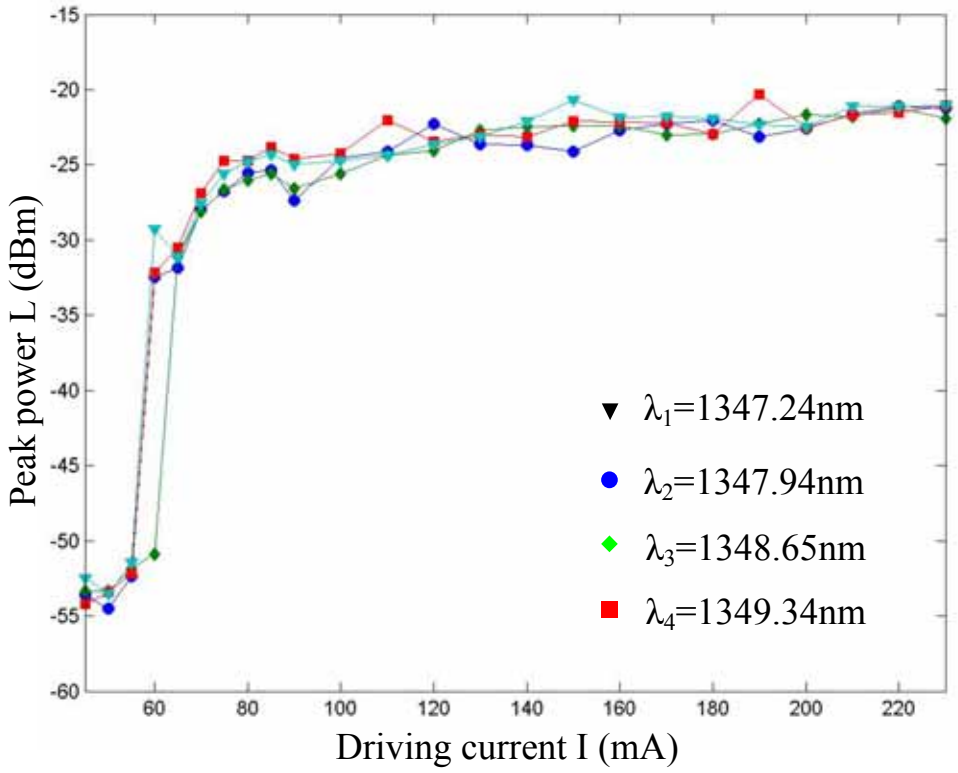

Fig. 2-10 L-I curves of the output laser with different driving current

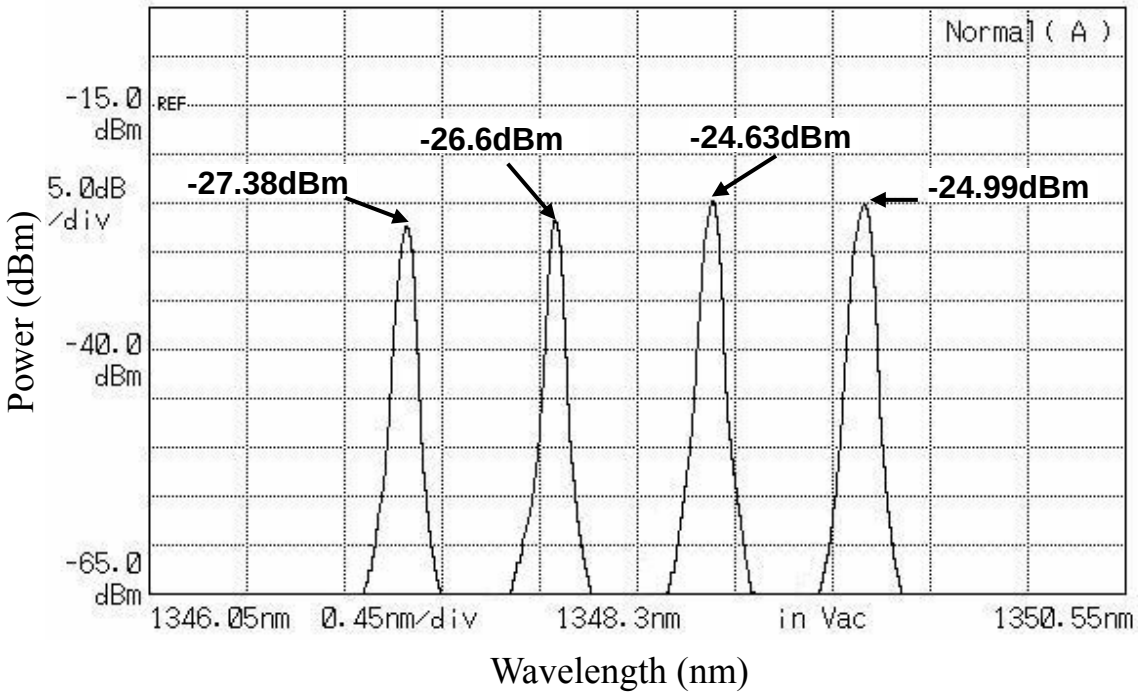

Fig. 2-11 The output lasing spectrum with driving current of SOA is 90mA

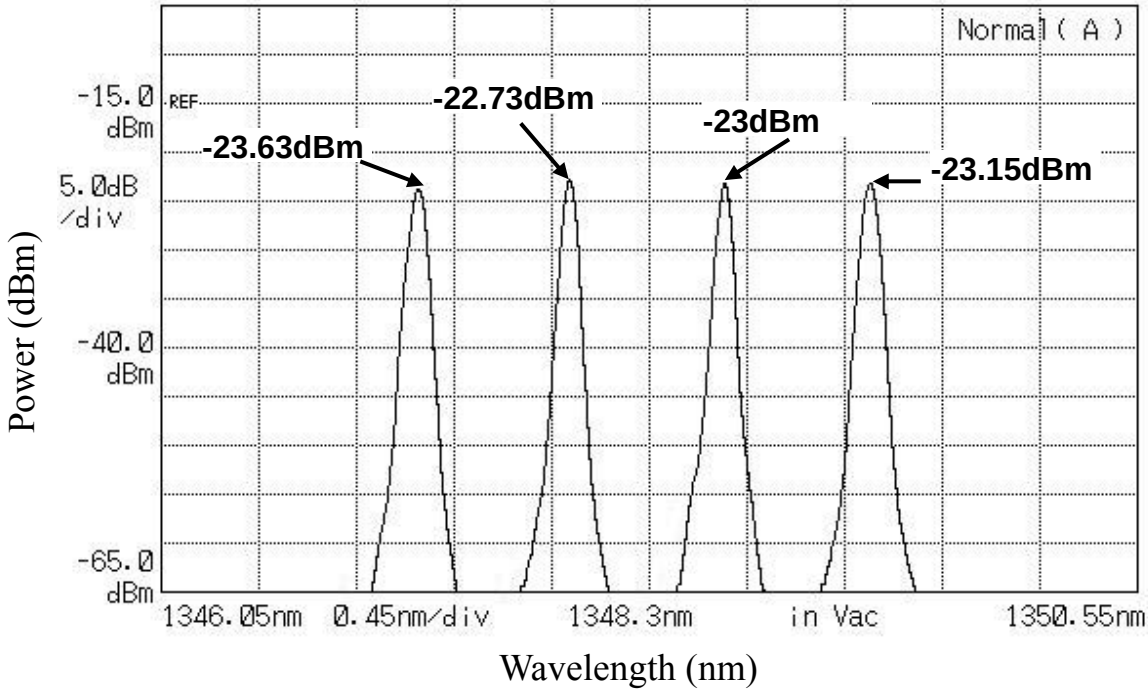

Fig. 2-12 The output lasing spectrum with driving current of SOA is 130mA

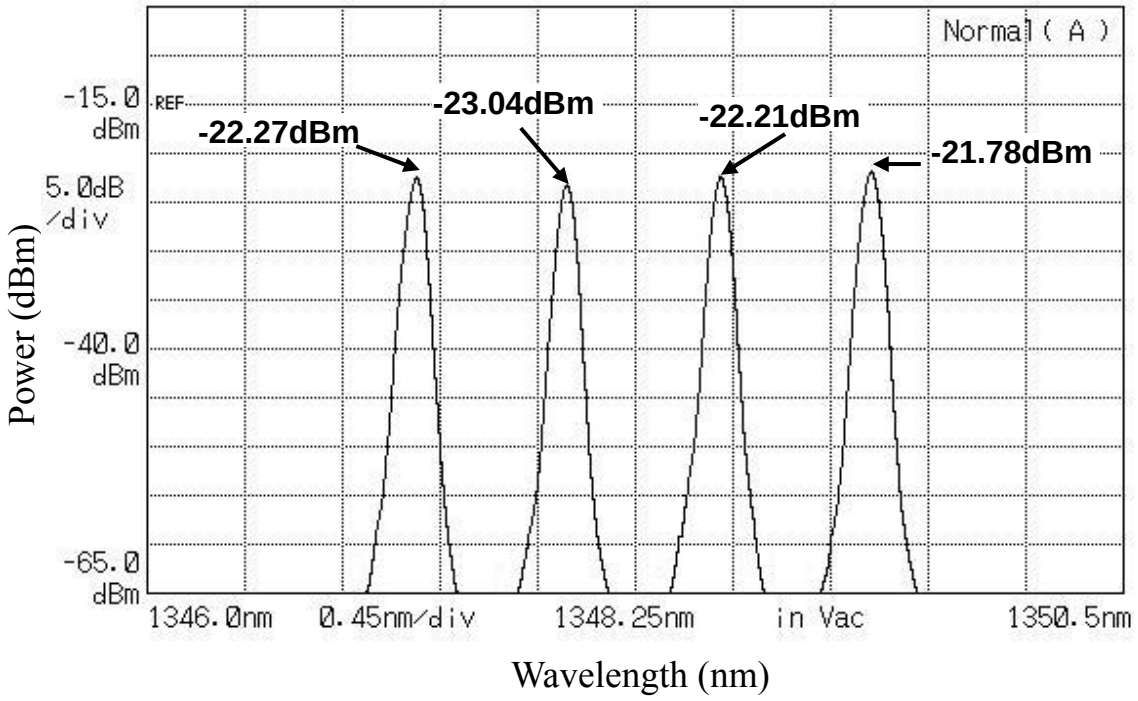

Fig. 2-13 The output lasing spectrum with driving current of SOA is 170mA

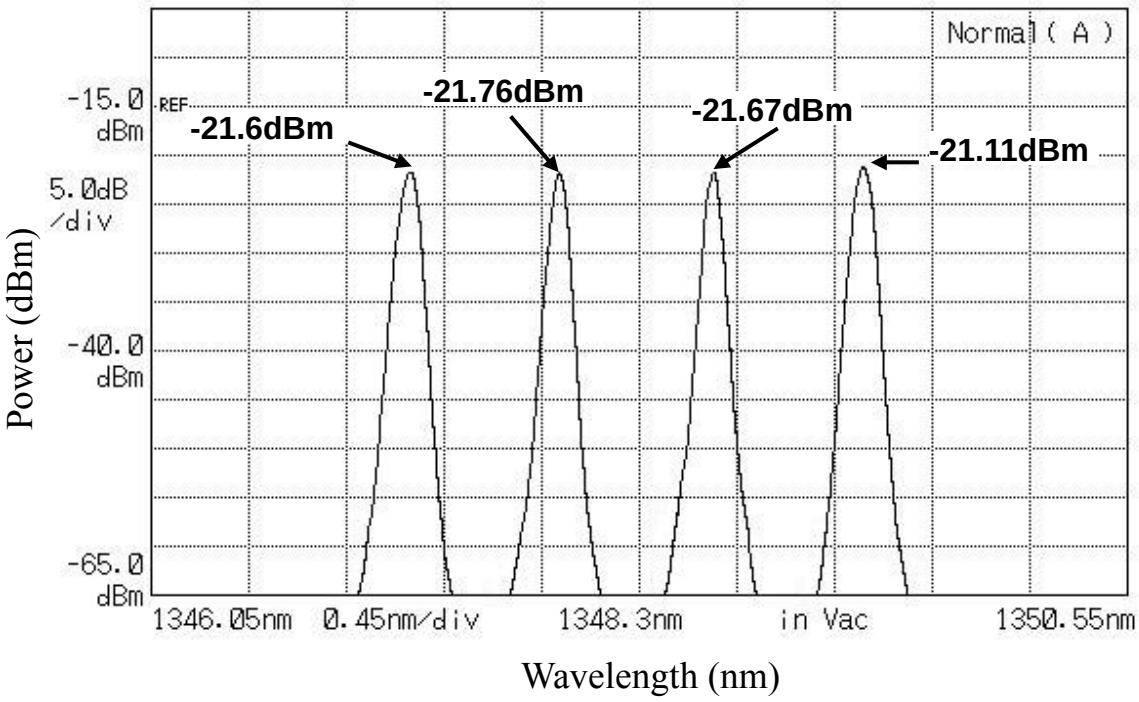

Fig. 2-14 The output lasing spectrum with driving current of SOA is 210mA

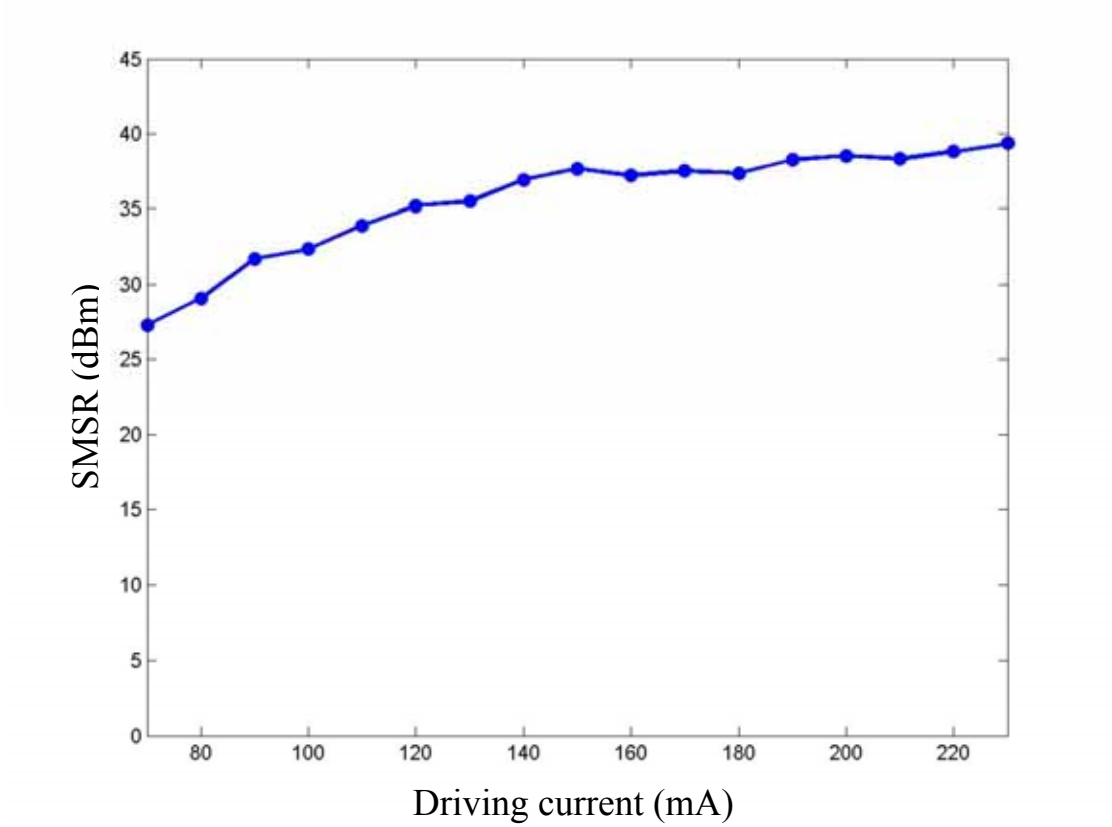

Fig. 2-15 The curve of SMSR versus driving current of SOA @ λ = 1347.24nm

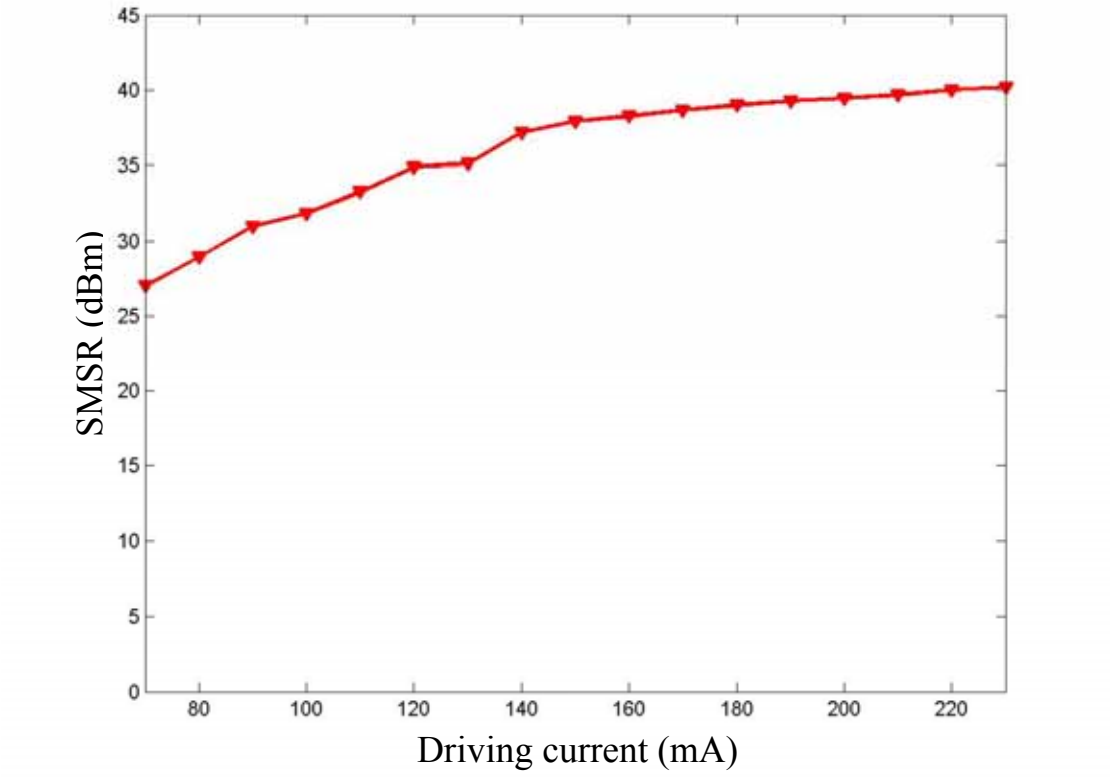

Fig. 2-16 The curve of SMSR versus driving current of SOA @ λ = 1347.94nm

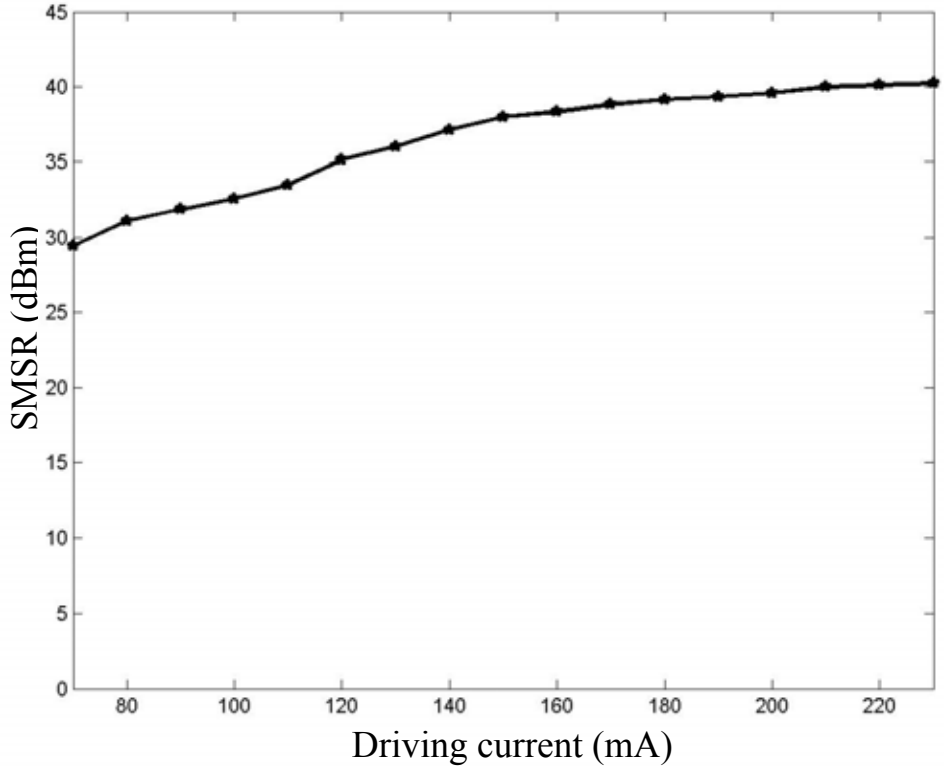

Fig. 2-17 The curve of SMSR versus driving current of SOA @ λ = 1348.65nm

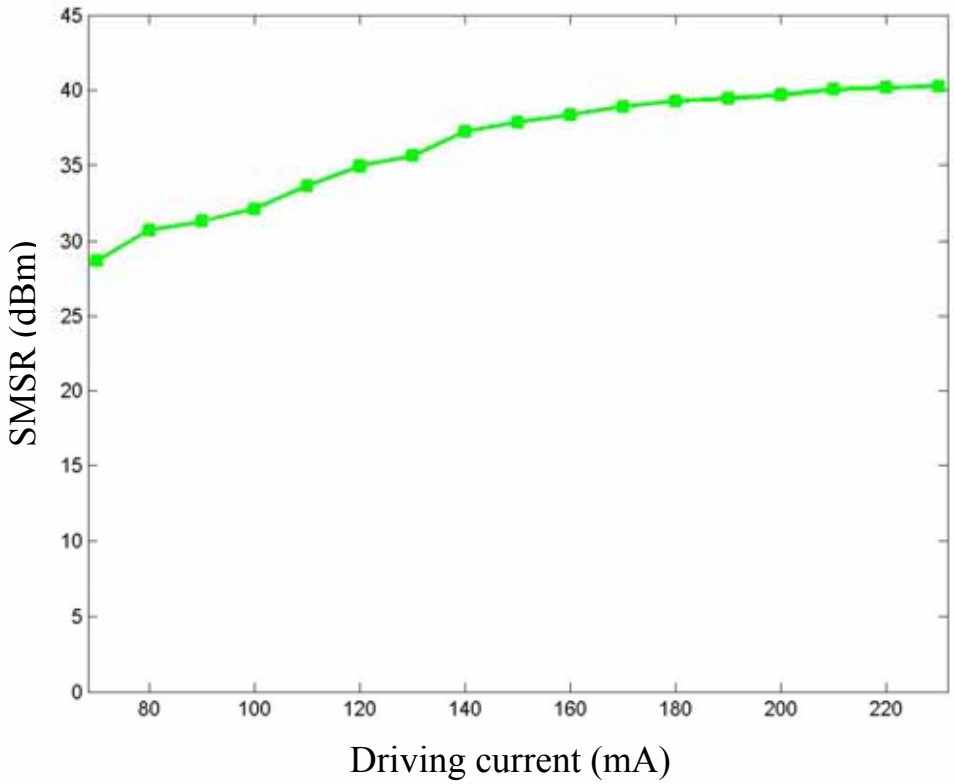

Fig. 2-18 The curve of SMSR versus driving current of SOA @ λ = 1349.34nm

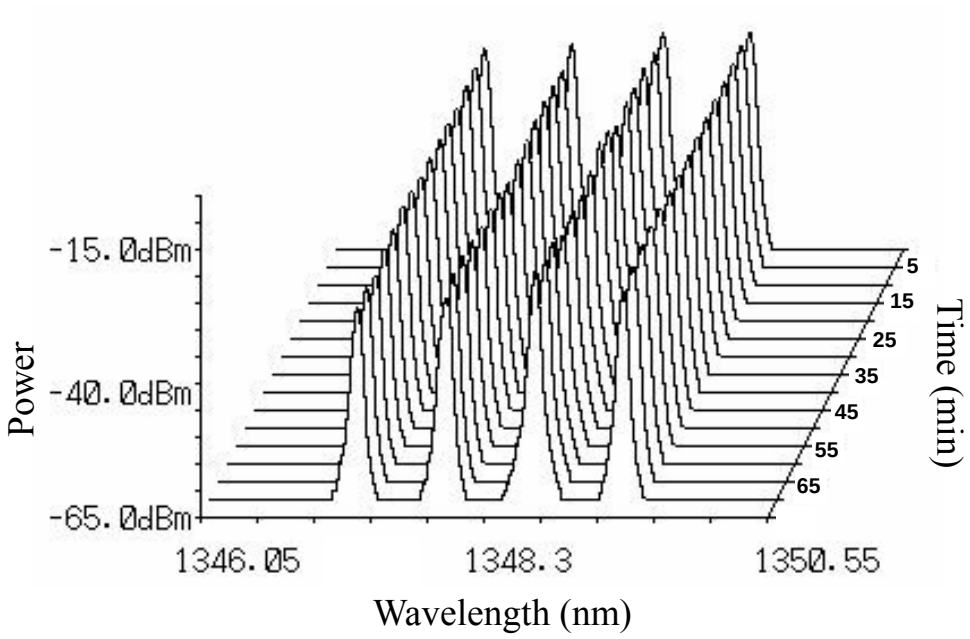

Fig. 2-19 (a) The optical spectrum of the stability of the output laser @ i_{SOA}= 90mA

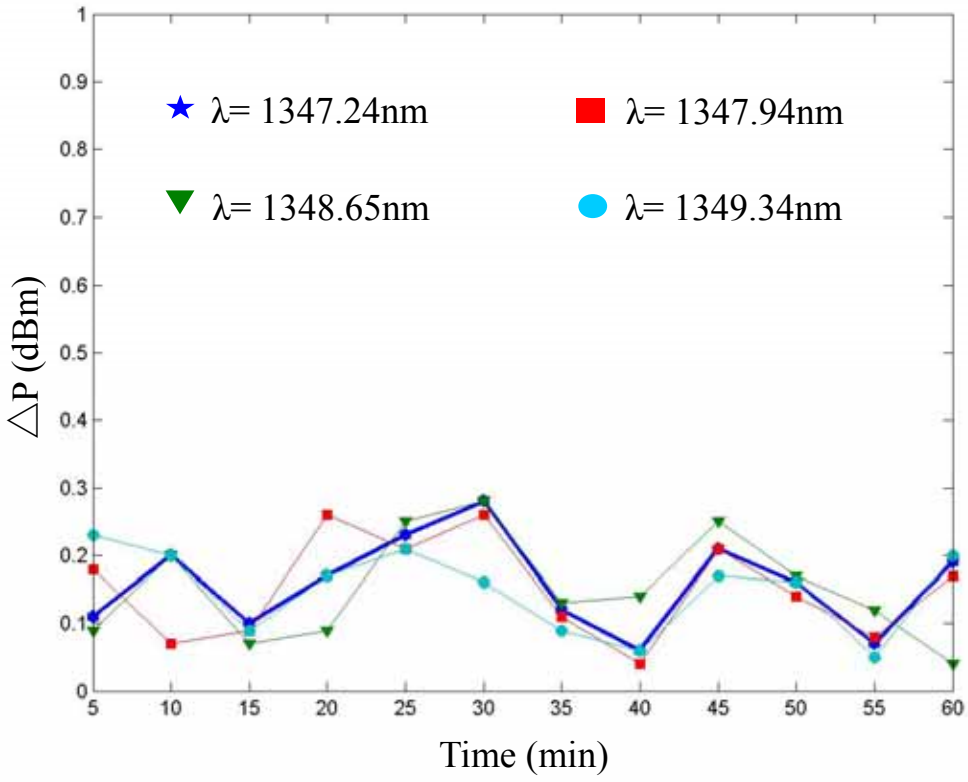

Fig. 2-19 (b) The relationship of the stability of the output laser @ i_{SOA}= 90mA

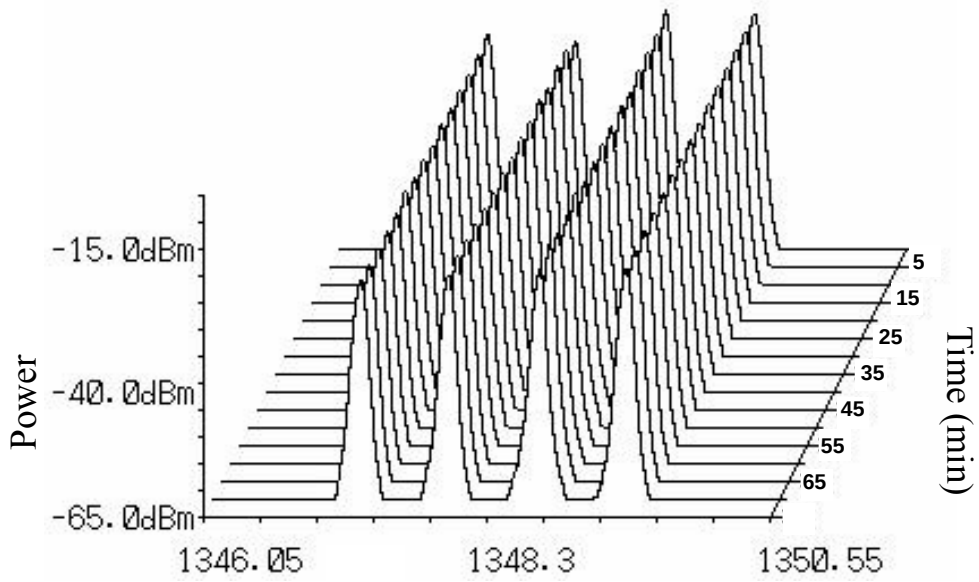

Fig. 2-20 (a) The optical spectrum of the stability of the output laser @ i_{SOA}= 130mA

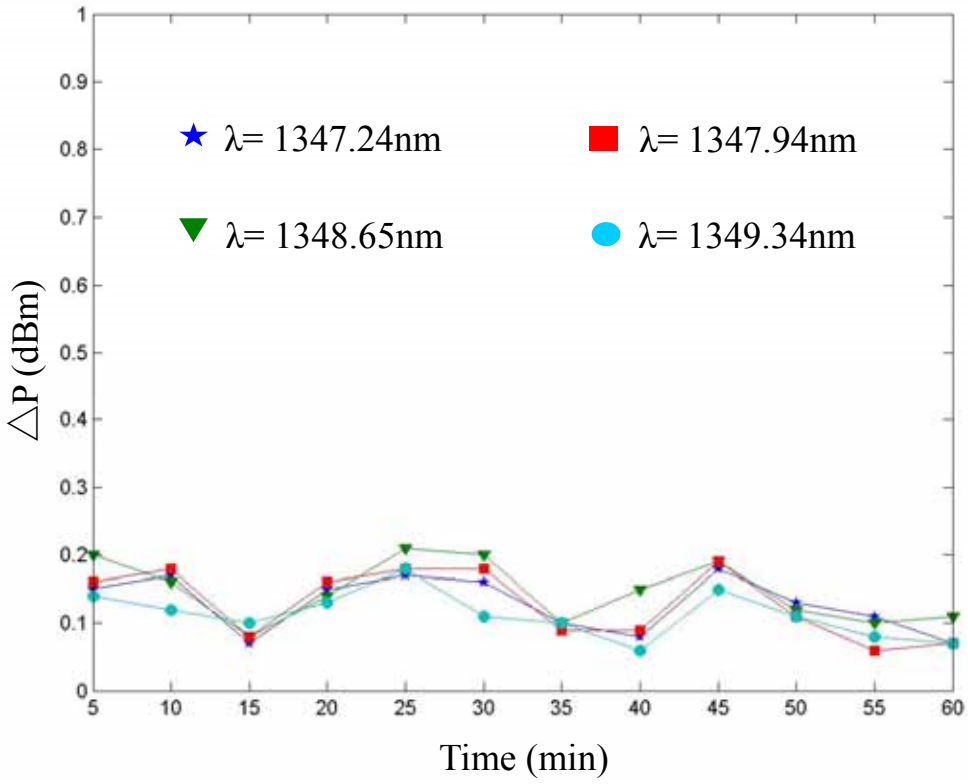

Fig. 2-20 (b) The relationship of the stability of the output laser @ i_{SOA}= 130mA

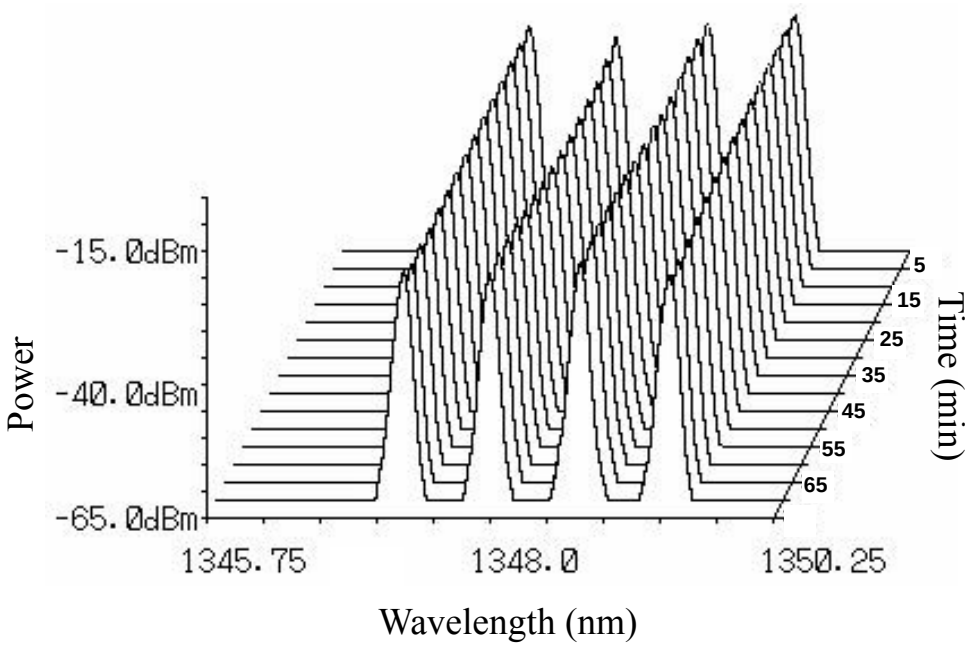

Fig. 2-21 (a) The optical spectrum of the stability of the output laser @ i_{SOA}= 170mA

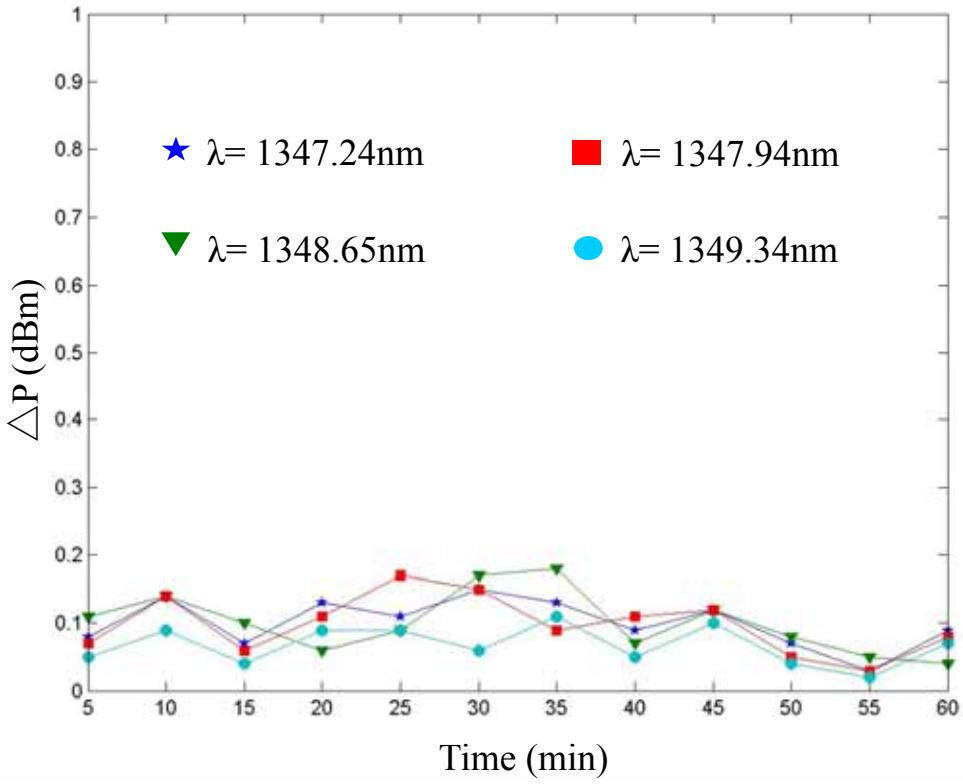

Fig. 2-21 (b) The relationship of the stability of the output laser @ i_{SOA}= 170mA

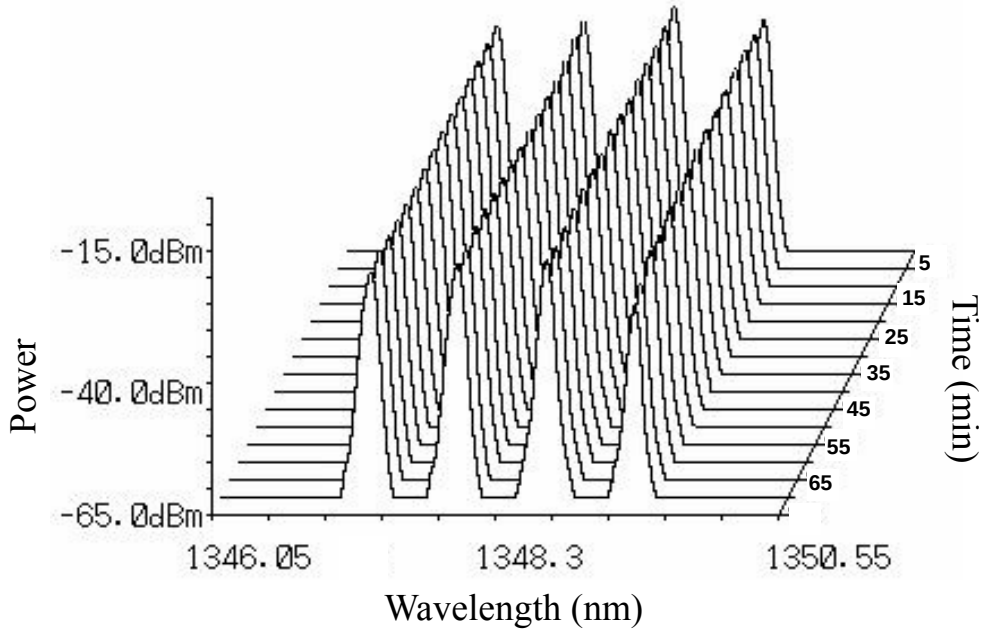

Fig. 2-22 (a) The optical spectrum of the stability of the output laser @ i_{SOA}= 210mA

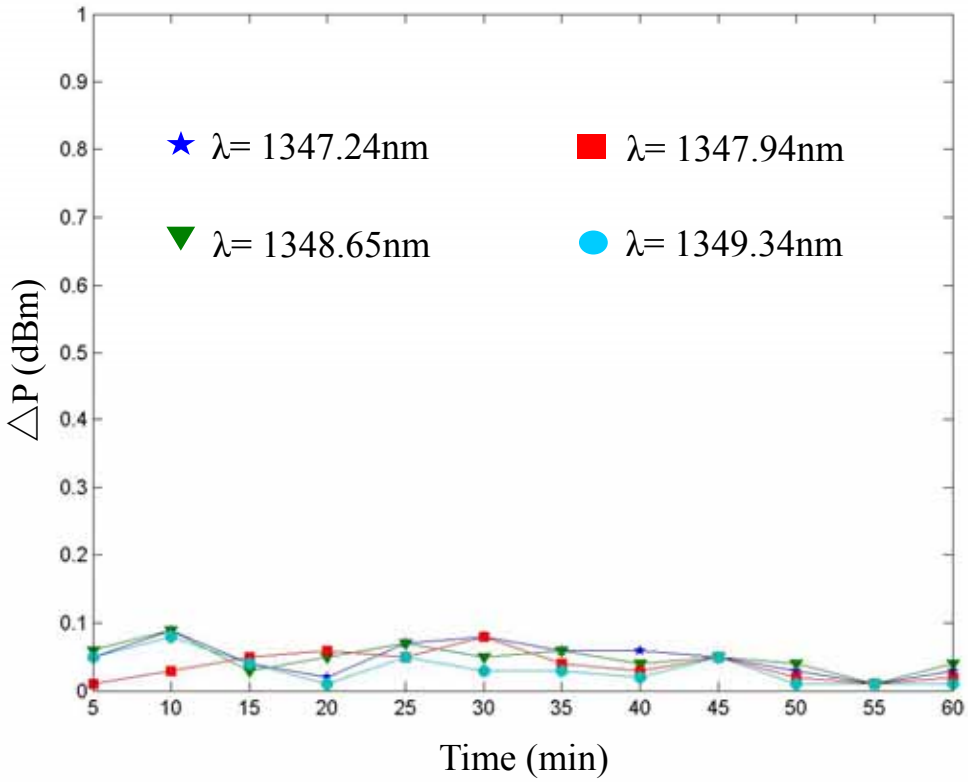

Fig. 2-22 (b) The relationship of the stability of the output laser @ i_{SOA}= 210mA

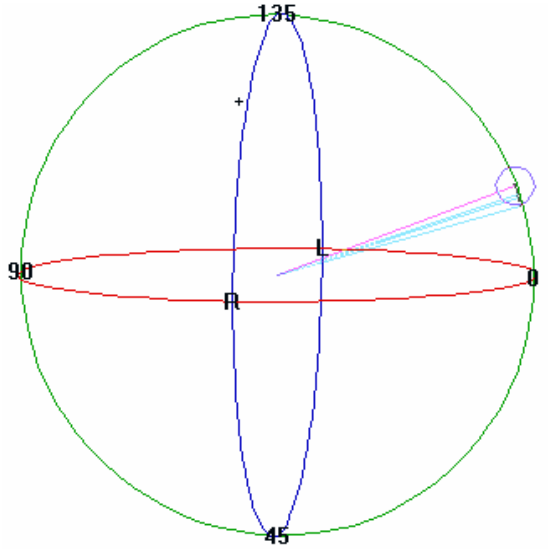

(a) Driving current = 90mA

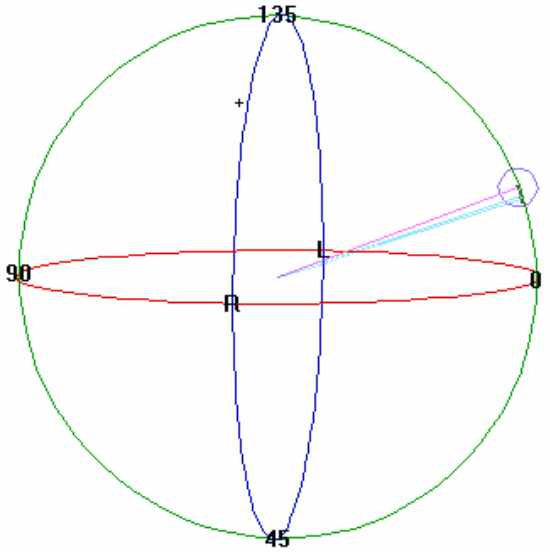

(b) Driving current = 130mA

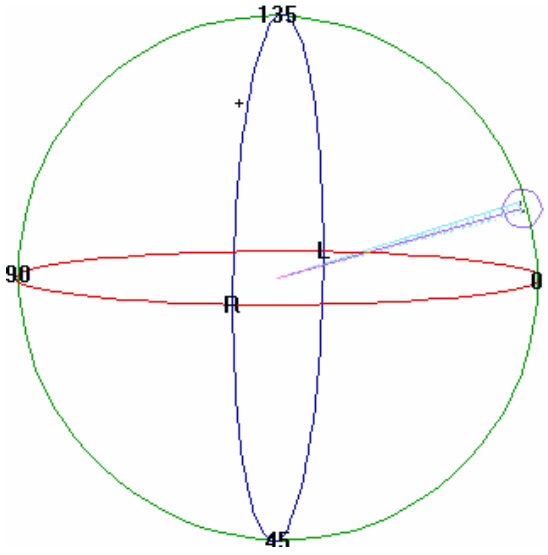

(c) Driving current = 170mA

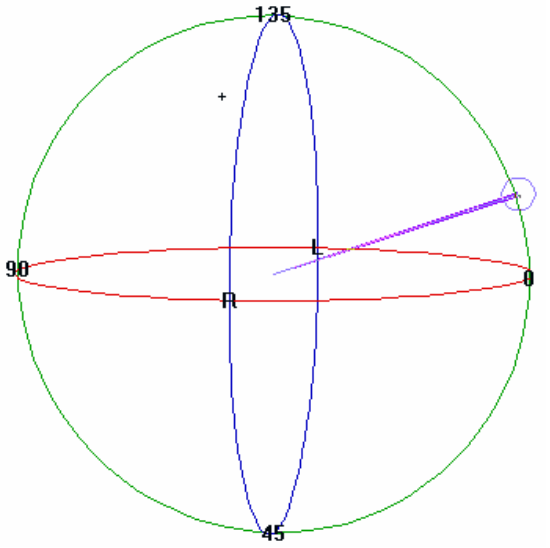

(d) Driving current = 210mA

Fig. 2-23 The polarization state measurement with different current of SOA @ λ =1347.24nm

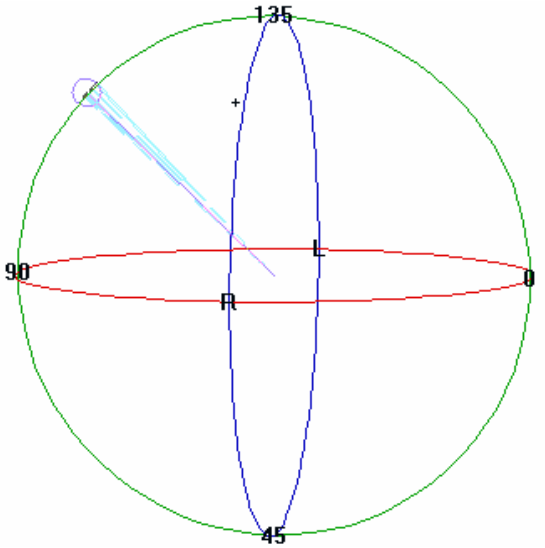

(a) Driving current = 90mA

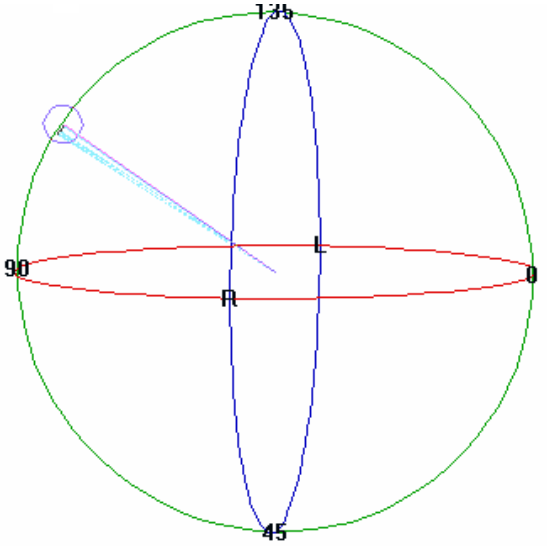

(b) Driving current = 130mA

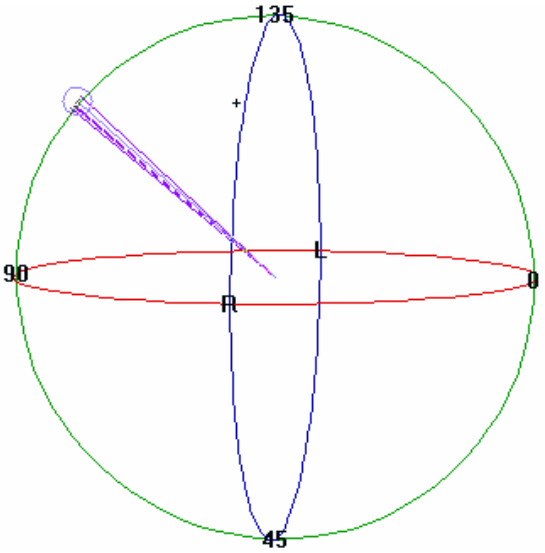

(c) Driving current = 170mA

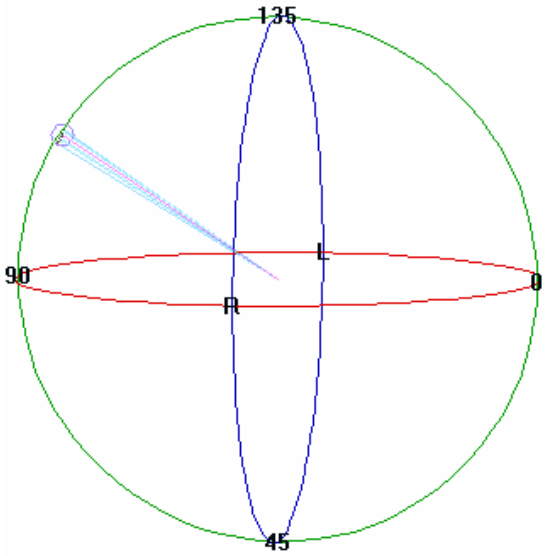

(d) Driving current = 210mA

Fig. 2-24 The polarization state measurement with different current of SOA @ λ =1347.94nm

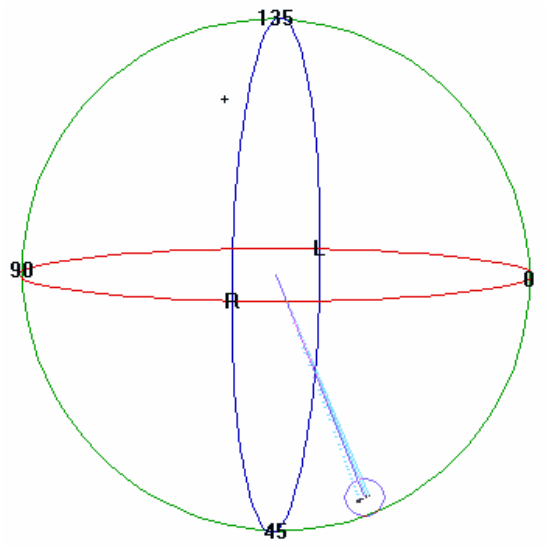

(a) Driving current = 90mA

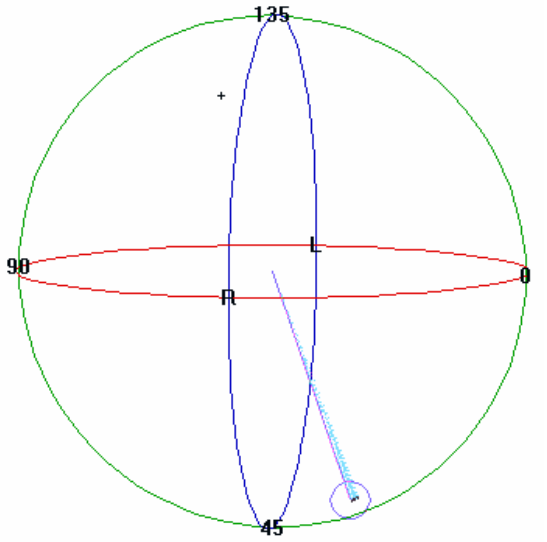

(b) Driving current = 130mA

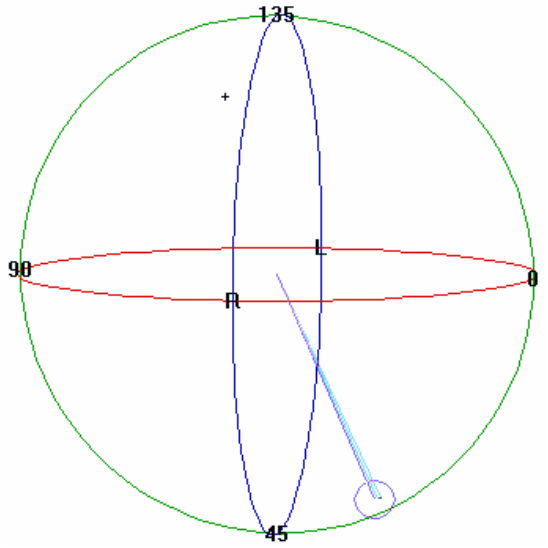

(c) Driving current = 170mA

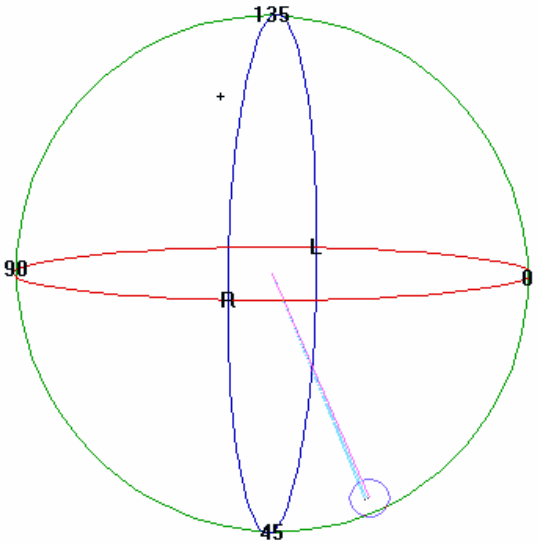

(d) Driving current = 210mA

Fig. 2-25 The polarization state measurement with different current of SOA @ λ =1348.65nm

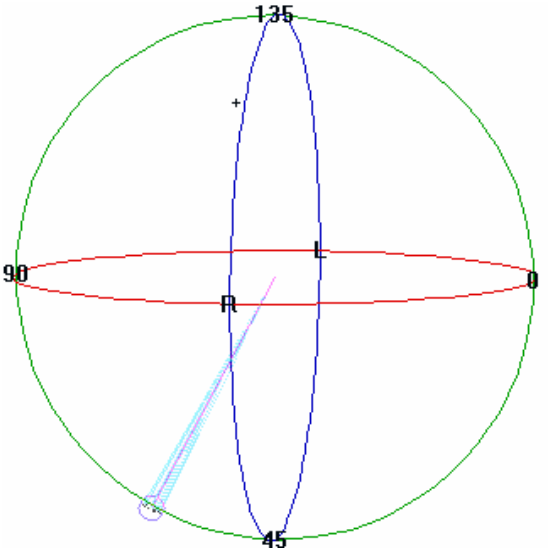

(a) Driving current = 90mA

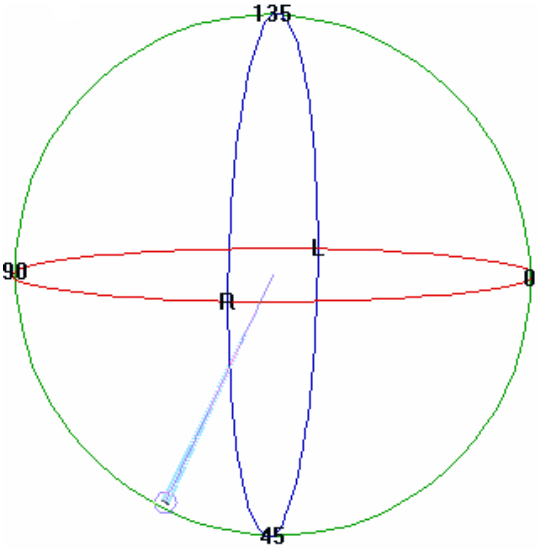

(b) Driving current = 130mA

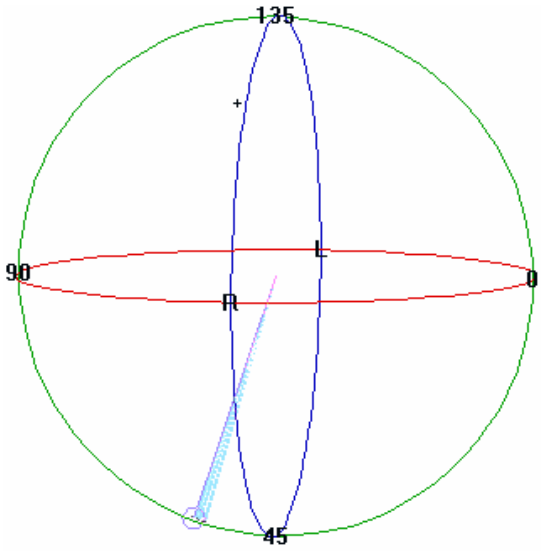

(c) Driving current = 170mA

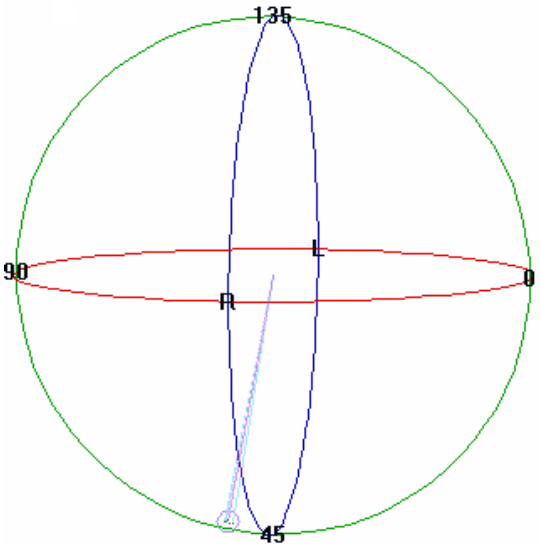

(d) Driving current = 210mA

Fig. 2-26 The polarization state measurement with different current of SOA @ λ =1349.34nm

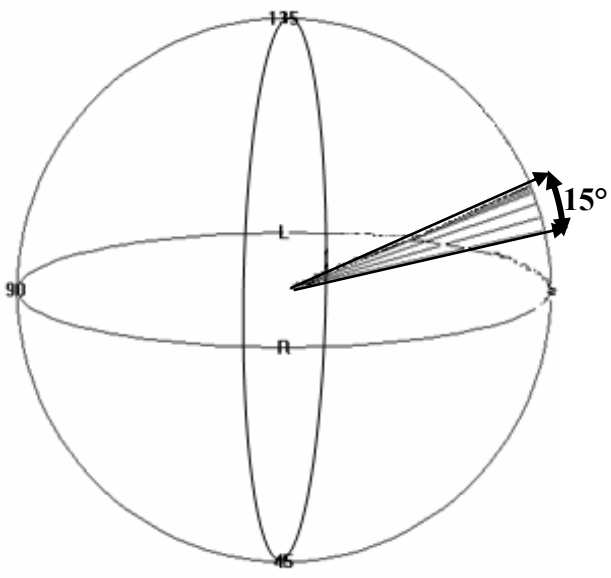

(a) Orientation variations of λ_1=1347.24nm

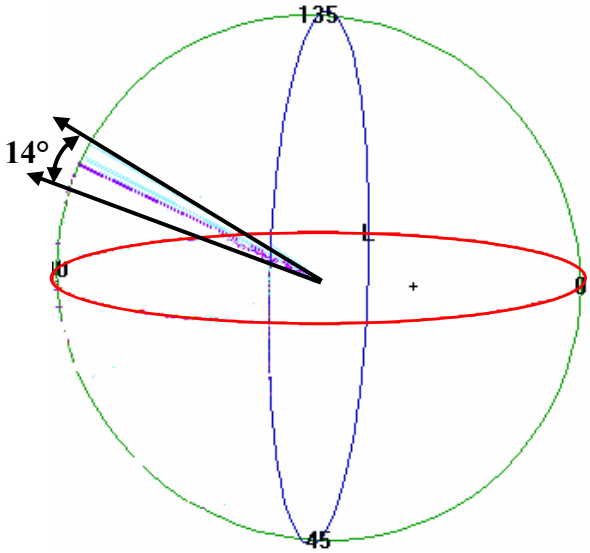

(b) Orientation variations of λ_2=1347.94nm

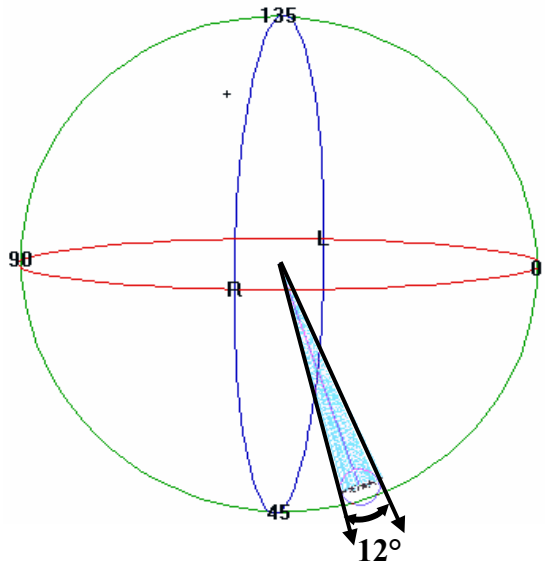

(c) Orientation variations of λ_3=1348.65nm

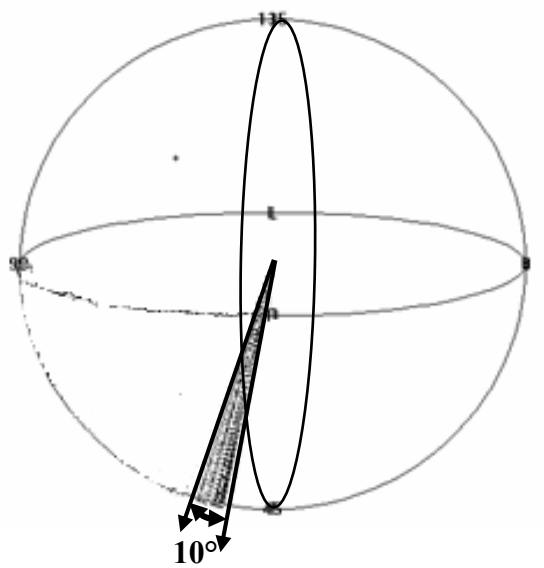

(d) Orientation variations of λ_4=1349.34nm

Fig. 2-27 The polarization state variation of the laser with turning the driving current of SOA from 80mA to 250mA

Specification	
Gain (G_{peak})	14.75dB@1309nm
Center wavelength (λ_{peak})	1310nm
Noise Figure (NF)	10dB
Optical bandwidth	50nm

Table 2-1 The specification of the 1.3μm SOA

Driving Current (mA)	Gain (dB)
110	5.45
130	8.48
150	10.6
170	12.01
190	12.86
210	13.67
230	14.13
250	14.75

Table 2-2 The relationship between the gain profile and driving current of 1.3μm SOA

Parameters		Values	
k (Coupling ratio)		0.9 or 0.5	
γ (Intensity loss of the coupler)		-0.1 dB	
L_1 (Fiber loop length at left hand side)		0.6 m	
L_2 (Fiber length including the Gain medium length)	L_{fiber} (Fiber length)	~1 m	1m
	$L_{gain\ material}$ (Gain medium length)		500×10^{-6}m
L_3 (Fiber loop length at right hand side)		0.8 m	
α(Field loss coefficient / Fiber Absorption)		Variable	
n (refractive index of the fiber)		1.46	
n_{air} (refractive index of the air)		1	
$n_{gain\ material}$ (refractive index of gain meterial)		3.4	
β (Propagation constant)		Variable	
g		Gain profile	

Table 2-3 The simulation parameters of the fiber resonator laser